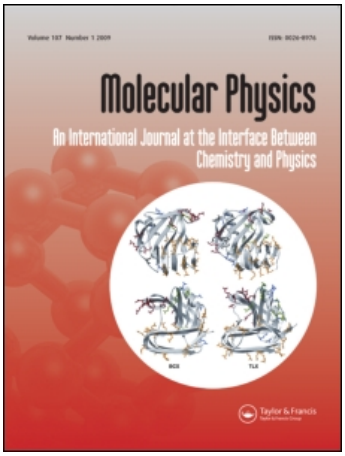

Molecular Physics
Publication details, including instructions for authors and subscription information:
http://www.informaworld.com/smpp/title~content=t713395160

Ro-vibrational spectra of C_2H_2 based on variational nuclear motion calculations

Andrea Urru[a]; Igor N. Kozin[b]; Giacomo Mulas[a]; Bastiaan J. Braams[cd]; Jonathan Tennyson[e]
[a] INAF-Osservatorio Astronomico di Cagliari, I-09012 Capoterra, (CA), Italy [b] STFC Daresbury Laboratory, Warrington, Cheshire, UK [c] Chemistry Department and Emerson Center for Scientific Computation, Emory University 1515 Dickey Drive, Atlanta, Georgia 30322, USA [d] Presently at the International Atomic Energy Agency, Vienna, Austria [e] Department of Physics and Astronomy, University College London, London WC1E 6BT, UK

Online publication date: 03 August 2010

To cite this Article Urru, Andrea , Kozin, Igor N. , Mulas, Giacomo , Braams, Bastiaan J. and Tennyson, Jonathan(2010) 'Ro-vibrational spectra of C_2H_2 based on variational nuclear motion calculations', Molecular Physics, 108: 15, 1973 — 1990
To link to this Article: DOI: 10.1080/00268976.2010.499858
URL: http://dx.doi.org/10.1080/00268976.2010.499858

Molecular Physics
Vol. 108, No. 15, 10 August 2010, 1973–1990

Taylor & Francis
Taylor & Francis Group

RESEARCH ARTICLE

Ro-vibrational spectra of C_2H_2 based on variational nuclear motion calculations

Andrea Urru[a]*, Igor N. Kozin[b], Giacomo Mulas[a], Bastiaan J. Braams[cd] and Jonathan Tennyson[e*]

[a]*INAF – Osservatorio Astronomico di Cagliari, Strada 54, Località Poggio dei Pini, I–09012 Capoterra, (CA), Italy;* [b]*STFC Daresbury Laboratory, Daresbury, Warrington, Cheshire, WA4 4AD, UK;* [c]*Chemistry Department and Emerson Center for Scientific Computation, Emory University 1515 Dickey Drive, Atlanta, Georgia 30322, USA;* [d]*Presently at the International Atomic Energy Agency, Vienna, Austria;* [e]*Department of Physics and Astronomy, University College London, Gower Street, London WC1E 6BT, UK*

(*Received 16 April 2010; final version received 4 June 2010*)

A published *ab initio*-based potential energy surface and newly constructed dipole moment surface of acetylene have been used to compute vibrational band intensities. The line intensity calculations employed the variational nuclear motion code WAVR4 for computation of wave functions and energy levels, and a newly developed code DIPOLE4 for computation of dipole transitions. Owing to the high computational cost of $J>0$ transitions using direct variational methods only $J=0$ and $J=1$ states and transitions have been computed variationally. The intensities of $J>1$ transitions were extrapolated from $J=0$ and $J=1$ using Hönl–London coefficients. The resulting effective rotational constants B and transition intensities are compared with experimental data for the $(3\nu_4+\nu_5)$ combination band, the ν_3 and the ν_5 fundamental band. The prospects of using this procedure for extensive calculations of a hot line list, important for cool stars and extrasolar planets are discussed.

Keywords: infrared spectra; variational; molecular opacity

1. Introduction

The infrared spectroscopy of the acetylene molecule C_2H_2 is important for atmospheric, planetary and astrophysical applications. Oxy-acetylene torches are also routinely used for cutting and welding metals [1] and indeed have been used as a spectroscopic source [2]. Acetylene is present as a trace constituent in the upper atmosphere of the giant planets where it comes from methane photodissociation. Thus the strong Q-branch of the ν_5 fundamental band, around 13.6 μm, has been observed in the emission spectra of the giant planets [3,4]. The stratospheric distribution of acetylene in Uranus was deducted from spectra obtained with the infrared space observatory (ISO) instrument [5]. In 1981, the first vertical profile of atmospheric C_2H_2 was obtained at wavelengths around 13.6 μm by Goldman *et al.* [6]. Acetylene, has been observed in the circumstellar shell of cool carbon stars such as IRC+10216, and in interstellar clouds, through spectra recorded in the 3 μm region of the ν_3 fundamental band [7,8], and in the 13.6 μm region of the ν_5 fundamental band [9,10]. Cool stars, known to be the most numerous, have spectra dominated by molecular absorption and, in particular for carbon stars (stars with a photospheric abundance of carbon greater than that of oxygen), one needs to consider triatomic species such as HCN and HNC [11], and C_3 [12]. For some dwarfs molecules larger than triatomics are known to form: methane and acetylene are thought to be particular important for carbon stars [12].

Given that the computed rotation–vibration line lists for triatomic species have contained between 10 and 500 million distinct transitions, line lists for polyatomic molecules will need to consider many billions of transitions. There remain very few comprehensive line lists for any species larger than triatomic [13–15]. Therefore the C_2H_2 molecule is interesting for testing theoretical approaches. We note that parallel to the present work a similar approach based on the MULTIMODE code [16] has been developed and applied to the CH_4 molecule by Warmbier *et al.* [15].

Acetylene has been studied extensively [17–19], at low vibrational energy (see for example Herman *et al.* [20] and references therein). There are fewer studies of acetylene at energies approaching the barrier to isomerisation and still fewer of vinylidene. The work most relevant to the understanding of intramolecular energy flow has been reviewed by Jacobson and Field [21]. Two of us recently developed a method for solving the problem of the calculation of the energy ro-vibrational levels and wave functions of a tetratomic molecule [22] and applied it to a study of

*Corresponding authors. Emails: aurru@oa-cagliari.inaf.it; j.tennyson@ucl.ac.uk

ISSN 0026–8976 print/ISSN 1362–3028 online

DOI: 10.1080/00268976.2010.499858
http://www.informaworld.com

acetylene/vinylidene vibrational levels [23]. There is very little theoretical work on general rotation–vibration, transition intensities for C_2H_2, the exception being the algebraic model calculations by Abbouti Temsamani *et al.* [24]. Developing a general first principles procedure calculation of intensities is the aim of the present work. For this purpose we developed a new code (DIPOLE4) designed to calculate the transition dipole moments of this molecule which we validated by comparison with available experimental data. Analytical expressions needed to develop the DIPOLE4 code and the existing data are described in Sections 2 and 3, with a comprehensive derivation given in the Appendix. Dipole moment surfaces and the calculations of energy levels and of transition dipole moments are given in Sections 4, 5 and 6 respectively. Section 7 compares our calculated transition intensities with experimental lists of ro-vibrational lines in two parallel bands. Section 8 presents the conclusions of the paper.

2. Transition intensity and selection rules

Given two specific energy levels of the molecule, the line strength $S(f \leftarrow i)$ of an electric dipole transition is defined as [25]

$$S_{(f\leftarrow i)} = \sum_{\Phi',\Phi} \sum_{A=X,Y,Z} |\langle \Phi' | \mu_A | \Phi \rangle|^2 \tag{1}$$

where Φ' runs over all states with energy E', Φ runs over all states with energy E, and μ_A is the component of the molecular dipole moment operator along the A axis ($A = X$, Y or Z) of the space fixed coordinate system with the origin at the molecular centre of mass. For $S_{(f\leftarrow i)}$ to be non-zero it must be invariant under all symmetry operations of the molecular symmetry group. This makes it possible to derive rigorous selection rules for transitions between states Φ' and Φ. More stringent selection rules can be derived if the vibrational motion is assumed harmonic or vibration and rotation is assumed separable. These rules however will be approximate and their accuracy will depend on validity of the initial assumptions.

For practical evaluation of $S_{(f\leftarrow i)}$, it is convenient to express space-fixed dipole components in terms of dipole projections on the molecule-fixed axes [25,26]

$$\mu_s^{(1,\sigma)} = \sum_{\sigma''=-1}^{1} [D^{(1)}_{\sigma,\sigma''}(\phi,\theta,\chi)]^* \mu_m^{(1,\sigma'')}, \tag{2}$$

where

$$\mu_m^{(1,\pm1)} = [\mp\mu_X - \mathrm{i}\mu_Y]/2^{1/2}; \quad \mu_m^{(1,0)} = \mu_Z. \tag{3}$$

So Equation (1) becomes

$$\begin{aligned} S_{(f\leftarrow i)} &= \sum_{\Phi'\Phi} \sum_{\sigma=-1}^{1} \left| \langle \Phi' | \mu_s^{(1,\sigma)} | \Phi \rangle \right|^2 \\ &= \sum_{\Phi'\Phi} \sum_{\sigma=-1}^{1} \left| \sum_{\sigma''=-1}^{1} \langle \Phi' | D^{(1)*}_{\sigma\sigma''} \mu_m^{(1,\sigma'')} | \Phi \rangle \right|^2. \end{aligned} \tag{4}$$

Moreover, for a linear molecule such as acetylene, the body-fixed wave functions are given as a linear combination of products of angular momentum eigenfunctions and vibrational basis functions expressed with respect to $3N-5$ internal coordinates. In general, any given state of the molecule can always be expressed in the form

$$\Phi(JMV) = \left(\frac{2J+1}{8\pi^2}\right)^{1/2} \sum_{k,v} c_v^{JkV} \phi_v^{Jk}(q) \mid JMk\rangle, \tag{5}$$

where V is a compound label of the vibrational state. The quantum numbers of the projection of the total angular momentum J onto the Z-axis of the space-fixed and onto the z-axis of the body-fixed frame are M and k respectively. Substituting Equations (5) into Equation (1), assuming isotropy of space (i.e. no magnetic fields) and making use of the algebraic properties of the Wigner coefficients one can obtain [27]

$$\begin{aligned} S_{(f\leftarrow i)} &= (2J'+1)(2J''+1) \\ &\times \left| \sum_{k',v',k'',v''} \sum_{\sigma''} (-1)^{k'} c_{v'}^{J'k'v'\star} c_{v''}^{J''k''v''} \begin{pmatrix} J' & 1 & J'' \\ k' & \sigma'' & (-k'') \end{pmatrix} \right. \\ &\left. \times \langle \phi_{v'}^{J',k'} \mid \mu_m^{(1,\sigma'')} \mid \phi_{v''}^{J'',k''} \rangle \right|^2. \end{aligned} \tag{6}$$

If the vibrational and rotational parts of the motion are well separated, it is possible [28] to choose the components of the wave functions so that they can be written more simply as

$$\Pi(JMV) = \left(\sum_v a_v^V \phi_v(q) \right) \left(\sum_k b^{Jk} | JMk \rangle \right). \tag{7}$$

In the limit of small displacements from equilibrium, this separation is exact. This separation is optimally obtained [27] using the embedding defined by the Eckart conditions [28]:

$$\sum_i m_i \hat{r}_{i,\mathrm{e}} \times \hat{r}_i = 0; \quad \sum_i m_i \hat{r}_i = 0, \tag{8}$$

where m_i is the mass and $\hat{r}_i$ the position ($\hat{r}_{i,\mathrm{e}}$ at equilibrium) of particle i. With the above equation, Equation (6) factorises into a product of two sums

which depend only on vibrational and rotational coordinates respectively [27], i.e.

$$S_{(f\leftarrow i)} = (2J'+1)(2J''+1) \times \left| \sum_{\sigma''} \sum_{v',v''} a_{v'}^{V'\star} a_{v''}^{V''} \langle \phi_{v'} \mid \mu_m^{(1,\sigma'')} \mid \phi_{v''} \rangle \times \sum_{k',k''} (-1)^{k'} b^{J'k'\star} b^{J''k''} \begin{pmatrix} J' & 1 & J'' \\ k' & \sigma'' & (-k'') \end{pmatrix} \right|^2. \quad (9)$$

For symmetry reasons the sum over σ is often restricted to only one value; thus at most one term at a time is non-zero for a given C_2H_2 transition. In this case Equation (9) can be rewritten as

$$S_{(f\leftarrow i)} = S_{\mathrm{Vib}}(V', V'') S_{\mathrm{Rot}}(J', J''), \quad (10)$$

where

$$S_{\mathrm{Vib}}(V', V'') = |\langle V'|\mu_m|V''\rangle|^2 = |\langle V'|\mu_m^{(1,\sigma)}|V''\rangle|^2 \quad (11)$$

and $S_{\mathrm{Rot}}(J', J'')$ are algebraic coefficients which are completely determined by the rotational quantum numbers of the levels involved in the transition and by the value of σ for which $\langle V'|\mu_m^{(1,\sigma)}|V''\rangle$ is not zero. The $S_{\mathrm{Rot}}(J', J'')$ are called the Hönl–London coefficients [29] and are denoted $L_{J'',\Delta J=J'-J''}$ below. Within this method, a transition will have intensity if the product $\langle V'|\mu_m^{(1,\sigma)}|V''\rangle$ is totally symmetric with respect to all symmetries of the molecule.

2.1. *Rotational selection rules and Hönl–London factors*

Below we list the relevant selection rules and Hönl–London coefficients for the case of a linear, symmetric molecule such as C_2H_2, for which the vibrational angular momentum is denoted by l. The general transition selection rules can be summerised as [30]:

(1) $\Delta l = 0$ with $l = 0$. This is the parallel transition of the $\Sigma^+ \rightarrow \Sigma^+$ type for stretching modes with only $P(\Delta J = -1)$ and R branches $(\Delta J = +1)$.
(2) $\Delta l = \pm 1$. This is a perpendicular transition type for bending modes such as $\Pi \rightarrow \Sigma$, $\Delta \rightarrow \Pi$, and so forth, with P and R branches $(\Delta J = \pm 1)$ and a strong Q branch $(\Delta J = 0)$.
(3) $\Delta l = 0$ with $l \neq 0$. These are transitions of the type $\Pi \rightarrow \Pi$, $\Delta \rightarrow \Delta$, and so forth with P and R branches $(\Delta J = \pm 1)$ and weak Q branches $(\Delta J = 0)$.

The terms parallel and perpendicular are used because the transition dipole moment is either parallel (μ_z) or perpendicular (μ_x and μ_y) to the molecular symmetry axis, conventionally labelled as the z-axis. By using the Hönl–London coefficients [29], the intensities of individual lines can be approximately reduced to a single band intensity which represents the intensity of the whole band. $L_{J,\Delta J}$ is defined as [30]

$$L_{J,\Delta J=-1} = \frac{(J - l\Delta l)(J - l\Delta l - 1)}{2J} \quad \text{(P-branch)}, \quad (12)$$

$$L_{J,\Delta J=0} = \frac{(2J+1)(J - l\Delta l)(J + l\Delta l + 1)}{(2J)(J+1)} \quad \text{(Q-branch)}, \quad (13)$$

$$L_{J,\Delta J=+1} = \frac{(J + l\Delta l + 2)(J + l\Delta l + 1)}{2(J+1)} \quad \text{(R-branch)}, \quad (14)$$

for perpendicular bands ($\Delta l = \pm 1$), and

$$L_{J,\Delta J=-1} = \frac{(J + l\Delta l)(J - l\Delta l)}{J}. \quad \text{(P-branch)}, \quad (15)$$

$$L_{J,\Delta J=0} = \frac{(2J+1)(l\Delta l)^2}{(J)(J+1)} \quad \text{(Q-branch)}, \quad (16)$$

$$L_{J,\Delta J=+1} = \frac{(J - l\Delta l + 1)(J + l\Delta l + 1)}{(J+1)} \quad \text{(R-branch)}, \quad (17)$$

for parallel bands ($\Delta l = 0$).

3. Existing data

Spectroscopic data for acetylene were introduced in the HITRAN database (molecule number 26) in the 1986 edition [31]. The 2004 HITRAN edition [32] and the recent 2008 HITRAN edition [33] contain essentially all available experimental data on the infrared spectra of the acetylene molecule. The 13.6 and 3 μm [34–38] spectral regions of interest are represented, using the work of Varanasi *et al.* [39] and Rinsland *et al.* [7] for both line positions and intensities. More than 670 line intensities of nine perpendicular bands of acetylene are measured in the 2.5 μm [40] spectral region and in the work of Lyulin *et al.* [41] the previous measurements of the line intensities of acetylene were extended in the 1.9 and 1.7 μm spectral regions.

Potential energy surfaces (PES) have been derived, from *ab initio* calculations, for an acetylene molecule spanning the acetylene and vinylidene minima and isomerisation barrier. A potential energy function for the ground state surface of C_2H_2 was constructed by Carter and Mills [42] in 1980 using a many-body expansion of the potential. Certain discrepancies in this potential were removed by Halonen *et al.* [43] who included the *ab initio* data due to Dykstra and Schaefer [44] on the vinylidene–acetylene transition state,

and also to reproduce a known barrier on the HC+CH dissociation pathway. The most accurate presently available potential energy surfaces were recently obtained by the Bowman group (see [45–48]). The final *ab initio* PES, due to work of Zou and Bowman [47], is an accurate, least-squares fit to nearly 10,000 symmetry-equivalent, *ab initio* electronic calculations obtained at the coupled-cluster singles, doubles (triples) CCSD(T) level of theory, with an aug-cc-pVTZ Gaussian basis set. This PES is used below. We note that more recently, a new semi-empirical potential energy surface was obtained by Xu *et al.* [48], based on the *ab initio* calculations of [47] with the addition of empirical scaling for the stretching coordinates. The parameters of the empirical scaling functions were determined to obtain the best fit of variational energy levels with respect to their experimental values.

4. Dipole moment surfaces

The dipole moment surface (DMS) for the present studies is a fit to a dataset of 17,410 calculations based on density functional theory using the Handy HCTH/147 functional [49] and Dunning's correlation-consistent polarised valence triple zeta (cc-pvtz) basis sets [50]. The calculations were carried out using the MOLPRO program package [51]. The nuclear configurations for the dipole moment dataset were obtained by sampling from molecular dynamics and diffusion Monte Carlo calculations using another separate fitted potential energy surface. The molecular dynamics calculations were run at energies up to break-up of the molecule and the diffusion Monte Carlo calculations were done at artificially reduced nuclear masses in order to sample high-energy regions of configuration space. Starting configurations were selected both in the acetylene and vinylidene regions of configuration space and additional sampling was done around the barriers to isomerisation. Further configurations were generated from fragment calculations for C_2H+H, CH+CH, CH_2+C and C_2+H_2; the two fragments being placed far apart to create an artificial C_2H_2 molecule for which the dipole is the sum of the fragment dipoles. Many high-energy configurations were thereby introduced into the dataset; however, the fitting uses a weighted root mean square (rms) minimisation criterion where the weight of a configuration at energy E relative to the global minimum is $(\delta_0/(E+\delta_0))(\delta_1/(E+\delta_1))$ with $\delta_0 = 0.1$ Hartree and $\delta_1 = 1.0$ Hartree. The factor involving δ_0 implies a smooth transition from an absolute to a relative error criterion around $E = 0.1$ Hartree and the factor involving δ_1 provides additional damping for configurations that have extremely high energy. The final dataset contains 14,167 configurations in the molecular region and 3243 fragmented configurations. There are 2556 configurations having energy in the range 0–0.1 Hartree relative to the global minimum, 5421 having energy in the range 0.1–0.2 Hartree, and the remainder have energy above 0.2 Hartree.

As in other work by one of us with the Bowman group, such as for the protonated water dimer [52], the dipole moment is represented using a functional form that is invariant under permutation of like nuclei. The functional form is based on a point-charge model:

$$\boldsymbol{\mu} = \sum_i w_i(X)\boldsymbol{x}(i), \tag{18}$$

where X denotes the molecular configuration, $w_i(X)$ is the effective charge on the ith nucleus (this effective charge depends on the entire configuration) and $\boldsymbol{x}(i)$ is the position vector of the ith nucleus. The effective charges are expanded in a set of basis functions, $w_i(X) = \sum_k c_k b_k(i, X)$, where b_k is the kth basis function, depending on the nuclear index i as well as on the configuration X, and the coefficients c_k are obtained by solving a weighted least-squares system with the dipole moment data on the right-hand side. The basis functions are polynomials in 'Morse variables' of the internuclear distances, $y(i,j) = \exp(-r(i,j)/\lambda)$, where λ was set to $2a_0$. The specific form of the basis functions is such as to make them covariant under interchange of identical nuclei; thus, if configuration X is transformed into X' by interchange of identical nuclei i and j then the pair $(b_k(i,X),\ b_k(j,X))$ is equal to the pair $(b_k(j,X'),\ b_k(i,X'))$. The construction of the basis function used tools of computational invariant theory [53] and the MAGMA computer algebra system [54,55]. As the basis functions depend ultimately on internuclear distances, they transform like scalars and so the fitted dipole moment $\boldsymbol{\mu}$ transforms like a vector; moreover, it is invariant under interchange of identical nuclei. The dipole moment is invariant under translation of the molecule subject to the condition $\sum_i w_i(X) = 0$ (appropriate for a neutral molecule), but in the present work this condition is not built into the basis, rather it is imposed as an additional constraint in the least-squares system, and is therefore not satisfied exactly. For that reason, in our calculations we placed the origin of the reference system coincident with the centre of mass of the nuclei.

The error in the fitted DMS is composed of *ab initio* error and fitting error. In order to assess the *ab initio* error we carried out a batch of calculations using a method that is presumed to be more accurate: finite field finite difference calculations of the dipole moment based on the coupled-cluster singles and doubles with

perturbative treatment of triples, CCSD(T), method and the aug-cc-pVTZ basis sets. A finite field of ± 0.005 au was used. The test configurations were obtained by running molecular dynamics at energy of 0.1 Hartree (21,947 cm^{-1}) relative to the acetylene global minimum, sampling from that run, and subjecting each sampled configuration to a random normal perturbation of half-width $0.05\,a_0$ for each Cartesian component of each nucleus. A sample of 895 configurations was obtained this way. Within this test dataset the root mean square of the norms of the RCCSD(T)/aug-cc-pVTZ dipoles is 0.4137 au, and we use that number as the scale for relative discrepancies. The root mean square norm of the vectorial difference between the hcth147/cc-pVTZ and the RCCSD(T)/aug-cc-pVTZ dipoles is 0.0195 au, which implies then a relative discrepancy of 4.7%. There is a slight systematic trend in the discrepancy as well: the average signed difference between the norm of the hcth147/cc-pVTZ dipole and the norm of the RCCSD(T)/aug-cc-pVTZ dipole is 0.0144 au, with the hcth147 dipole being the larger one. This amounts to a difference of 3.5%. We conclude that the hcth147/cc-pVTZ is rather good. Indeed, the discrepancy with RCCSD(T)/aug-cc-pVTZ is significantly larger for two other plausible methods that we considered. For the B3LYP density functional and aug-cc-pVTZ basis we find an rms norm of the vectorial difference to the RCCSD(T) dipole of 0.0243 au (5.9%) and an average signed difference between the norms of 0.0198 au (4.9%), while for the MP2 method and the aug-cc-pVTZ basis the two characteristic discrepancies are 0.109 au (26%) and 0.0934 au (23%).

The fitting error was assessed two ways: by comparison of the fitted surface with the original data and by comparison with the newly generated independent dataset described above. With respect to the original dataset the rms norm of the dipole fitting error is 0.0055 au over the subset of data that have energy in the range 0–0.1 Hartree relative to the global minimum (2556 configurations) and 0.0142 au over the subset of data that have energy in the range 0.1–0.2 Hartree relative to the global minimum (5421 configurations). With respect to the hcth147/cc-pVTZ *ab initio* calculations for the new independent dataset the rms norm of the dipole fitting error is 0.0044 au over all configurations. Thus, according to this test the rms fitting error is 1.1% relative to the rms of the norms of the RCCSD(T)/aug-cc-pVTZ dipoles (0.4137 au as described above).

5. Calculations

Our goal is ultimately to calculate detailed lists of ro-vibrational transitions, including energies and intensities, among accurate states obtained via variational methods. As a first step we perform variational calculations to obtain rotation-less states (i.e. $J=0$) and obtain purely vibrational transitions. This greatly reduces the computational cost, while still enabling us to validate the newly developed part in the codes we used. However it should be understood that some vibrational states, namely those with non-zero vibrational angular momentum, cannot be represented with a basis set composed only of states with zero total angular momentum: levels, and transitions involving them, are simply not computed starting from $J=0$. Therefore we calculated ro-vibrational energies for $J=1$ and $J=2$ as well. This notably includes fundamental bending transitions, since for them the upper state has vibrational angular momentum $l=\pm 1$. Only overtones and combination bands of bending transitions can be computed, i.e. those in which (in the harmonic approximation) the occupation numbers of bending modes change by an even number (i.e. at least 2).

The computer program WAVR4 [22] calculates the bound ro-vibrational levels and wave functions of a tetratomic system based on the well-established technique of sequential diagonalisation and truncation [56]. The theoretical framework has been described before [22,23], so in the present section we only describe its specific implementation.

The present study uses orthogonal, HC–CH diatom–diatom coordinates which correspond to traditional valence coordinates in the limit that masses of atoms 1 and 4 are small compared to those of atoms 2 and 3. The angular coordinates are treated using a finite basis representation (FBR) based on a product of spherical harmonics. A discrete variable representation (DVR) based on a Morse-oscillator-like one is used for the radial coordinates [57]. Matrix elements are computed using an efficient Gaussian quadrature in the angular coordinates and the DVR approximation in the radial coordinates. The full basis is therefore a product of the FBR angular basis and a radial DVR basis. The solution of the secular problem is carried through a series of intermediate diagonalisations and truncations. All calculations reported were performed using the recent *ab initio* potential of Zou and Bowman [47]. The calculations were carried out on an Intel Xeon cluster at Daresbury Laboratory. Each node of the 32 node cluster comprised two dual-core Xeon 5160 3.0 GHz processors with 8 GBytes of RAM. The final wave function calculations were all for total angular momentum $J=0$ and $J=1$ and used six radial functions in each CH coordinate and nine radial functions in the CC coordinate. The parameters used for CH stretching Morse-oscillator-like functions were $r_e = 1.164$ Å, $w_e = 2900\,cm^{-1}$ and $D_e = 36000\,cm^{-1}$; the parameters

Table 1. Calculated vibrational band origins E_1^{th} and zero point energy ($ZPE = 5715.5$), comparison with experimental data E^{exp} [20,59,60]. Also given is the value of the rotational constant $\langle B^{\text{th}} \rangle$ which is compared to the experimental values $\langle B^{\text{exp}} \rangle$ [59].

	Assignment								
N°	ν_1,	ν_2,	ν_3,	$\nu_4^{l_4}$,	$\nu_5^{l_5}$	E^{th} (cm^{-1})	E^{exp} (cm^{-1})	$\langle B^{\text{th}} \rangle$ (cm^{-1})	$\langle B^{\text{exp}} \rangle$ (cm^{-1})
0	0,	0,	0,	0^0,	0^0	5715.5		1.164	1.177
1	0,	0,	0,	1^1,	0^0	602.2	612.9	1.166	1.178
2	0,	0,	0,	0^0,	1^1	722.2	730.3	1.169	1.179
3	0,	0,	0,	2^0,	0^0	1203.5	1230.8	1.164	1.179
4	0,	0,	0,	1^1,	1^{-1}	1311.6	1328.1	1.167	1.180
5	0,	0,	0,	1^1,	1^1	1325.7	1347.5	1.166	1.180
6	0,	0,	0,	0^0,	2^0	1448.6	1449.0	1.164	1.181
7	0,	0,	0,	3^1,	0^0	1812.5	1855.7	1.168	1.181
8	0,	1,	0,	0^0,	0^0	1950.7	1974.3	1.157	1.170
9	0,	0,	0,	4^0,	0^0	2419.0	2487.0	1.175	1.182
10	0,	0,	0,	3^1,	1^{-1}	2519.5	2560.6	1.172	1.183
11	0,	0,	0,	2^2,	2^{-2}	2632.1	2648.2	1.170	1.184
12	0,	0,	0,	2^0,	2^0	2675.9	2683.8	1.169	1.184
13	0,	0,	0,	1^1,	3^{-1}	2772.0	2757.8	1.168	1.185
14	0,	0,	0,	0^0,	4^0	2922.3	2879.9	1.165	1.186
15	0,	1,	0,	2^0,	0^0	3143.5	3180.8	1.163	1.173
16	0,	0,	1,	0^0,	0^0	3241.1	3316.9	1.160	1.185
17	0,	1,	0,	1^1,	1^{-1}	3254.3	3281.9	1.159	1.185
18	1,	0,	0,	0^0,	0^0	3371.1	3372.4	1.157	1.170
19	0,	1,	0,	0^0,	2^0	3379.2	3420.5	1.157	1.175
20	0,	0,	0,	6^0,	0^0	3642.6	3767.0	1.180	1.185
21	0,	0,	0,	5^1,	1^{-1}	3735.0	3818.4	1.178	1.186
22	0,	0,	0,	4^2,	2^{-2}	3839.6	3884.0	1.176	1.187
23	0,	0,	1,	1^1,	0^0	3867.7	3898.3	1.175	1.174
24	0,	2,	0,	0^0,	0^0	3886.0	3933.8	1.174	1.164
25	0,	0,	0,	4^0,	2^0	3911.9	3940.3	1.174	1.187
26	0,	0,	0,	2^2,	4^{-2}	4096.2	4060.0	1.171	1.188
27	0,	0,	0,	2^0,	4^0	4170.6	4124.6	1.169	1.188
28	0,	1,	0,	4^0,	0^0	4349.5	4415.6	1.168	1.176
29	0,	0,	0,	0^0,	6^0	4406.2	4293.1	1.166	1.190
30	0,	0,	1,	2^0,	0^0	4417.7	4489.1	1.164	1.175
31	0,	1,	0,	3^1,	1^{-1}	4447.3	4488.9	1.165	1.167
32	0,	0,	1,	1^1,	1^{-1}	4525.3	4609.3	1.162	1.175
33	1,	0,	0,	2^0,	0^0	4546.6	4570.0	1.163	1.173
34	0,	1,	0,	2^0,	2^0	4595.6	4634.4	1.162	1.178
35	1,	0,	0,	1^1,	1^{-1}	4656.5	4673.6	1.160	1.174
36	0,	1,	0,	1^1,	3^{-1}	4691.1	4710.7	1.162	1.177
37	1,	0,	0,	0^0,	2^0	4803.5	4800.2	1.158	1.174
38	0,	1,	0,	0^0,	4^0	4834.2	4848.9	1.158	1.179
39	0,	0,	0,	8^0,	0^0	4871.0	5068.5	1.176	1.188
40	0,	0,	1,	3^1,	0^0	5094.8	5102.8	1.181	1.176

for CC stretching were $r_e = 1.4135$ Å, $w_e = 2000\,\text{cm}^{-1}$ and $D_e = 55{,}000\,\text{cm}^{-1}$. The bending basis set was defined by $j_{\max} = l_{\max} = 26$ and $k_{\max} = 7$. These quantum numbers defined 4460 bending functions which are totally symmetric with respect to the inversion. Thus the total size of the primitive basis set was 1,445,040. To contract this basis set, up to 300 optimised bending functions were selected for each radial grid point during phase one with an upper energy cut-off of $30{,}000\,\text{cm}^{-1}$ and up to 450 functions during phase two with an energy cut-off of $30{,}000\,\text{cm}^{-1}$. The computation of all 300 vibrational (phase three) states and of all 600 (phase four) ro-vibrational states took a total of 220 h on a node of the 'cseem64t' cluster. The zero-point energy (ZPE) and the lowest 40 excited states with an energy cut-off of $5000\,\text{cm}^{-1}$ are presented in Table 1. Table 1 also gives the values of the rotational constant $\langle B \rangle$ for each state. The complete list of calculated energy states and of the effective rotational constant are available online [58].

6. Ro-vibrational band intensities

A new code, DIPOLE4, was developed to perform calculations of dipole transition intensities using the wavefunctions produced by WAVR4. The code can be

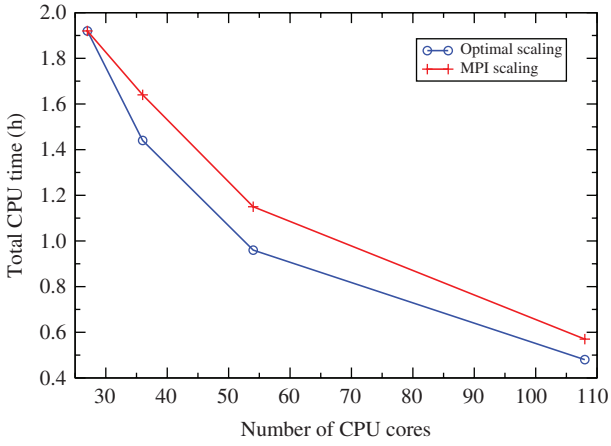

Figure 1. Running times for a large DIPOLE4 code run, MPI version, with varying numbers of CPU cores. The blue line shows perfect linear scaling extrapolated from the run using the smallest number of processors (27 CPU cores). The red line shows real running times for 27, 36, 54 and 108 CPU cores. [This figure can be viewed in colour online.]

used to perform direct calculations of dipole transitions $S_{(f\leftarrow i)}$ between ro-vibrational states. The details and all relevant formulae including their derivation are presented in Appendix 1. The calculation of the integrals proceeds in two stages [61]. In the first stage, the wave functions produced by WAVR4 code are converted back to the primitive basis set ϕ^{α} and the results are stored on disk. This allows more efficient calculation of the integrals and reuse of converted wave functions. In the final stage, the DIPOLE4 code reads converted wave functions, builds a matrix representation of the integrand in the primitive basis and performs computation of integrals involving all possible initial and final states. All steps of the final stage, apart from the first, are performed as a loop over the three-dimensional radial grid which allows efficient parallelisation. Furthermore, since we operate on vectors and matrices larger than typical cache, vector–matrix operations must be avoided due to their low efficiency. Therefore all the integrals are computed simultaneously only through matrix–matrix multiplications. Intermediate results are accumulated in a matrix of the size equal to the number of initial times final states.

For a parallel implementation the intermediate matrices reside on parallel processors and no communication is necessary during the computation; only a final reduction to the transition matrix is required at the end. In this case, since dynamic load balancing at run time does not offer particular advantages, we chose to use MPI. Since the parallelisation strategy uses processors-to-grid mapping, the best load balancing is achieved by using a number of processors which is a divisor of the total radial grid size. In our case, since we used a grid with $6 * 6 * 9 = 324$ points, 'good' numbers of processors are 162, 108 etc. Figure 1 shows the scaling properties of a large run of the DIPOLE4 code with different numbers of processing units, ranging from 27 to 108 cores. While scaling is not perfect, presumably due to overheads in partitioning the problem among jobs and collecting the results, it is

Table 2. A sample of the $J=0\Rightarrow J=0$ parallel transitions having non-zero intensity. Columns are, from left to right: number of the vibrational states involved, calculated vibrational energy difference, and calculated vibrational band intensity $S_{\mathrm{Vib}}(V', V'')$. See Table 1 for full vibrational labels and levels. Powers of 10 are given in parenthesis.

Transition	ΔE cm^{-1}	Line str. (e Å)^2
$1\rightarrow 3$	1311.5770	1.0(−3)
$1\rightarrow 7$	2519.4822	2.5(−7)
$1\rightarrow 10$	2772.0035	7.0(−8)
$1\rightarrow 13$	3241.0504	7.9(−4)
$1\rightarrow 14$	3254.3348	1.5(−3)
$1\rightarrow 22$	3955.6108	1.1(−10)
$1\rightarrow 29$	4417.7154	2.3(−6)
$1\rightarrow 30$	4447.3147	2.8(−7)
$1\rightarrow 35$	4656.4795	2.9(−7)
$1\rightarrow 36$	4671.1114	7.6(−8)
$1\rightarrow 37$	4691.0767	8.4(−9)
$2\rightarrow 3$	108.0469	7.7(−4)
$2\rightarrow 7$	1315.9521	1.8(−3)
$2\rightarrow 10$	1568.4734	2.1(−9)
$2\rightarrow 13$	2037.5203	6.6(−9)
$2\rightarrow 14$	2050.8047	1.0(−5)
$2\rightarrow 18$	2531.4690	1.5(−6)
$2\rightarrow 22$	2752.0807	3.0(−8)
$2\rightarrow 23$	2796.1914	6.0(−8)
$2\rightarrow 29$	3214.1853	1.7(−3)
$2\rightarrow 30$	3243.7846	1.9(−4)
$2\rightarrow 35$	3452.9494	2.1(−6)
$2\rightarrow 36$	3467.5813	8.5(−7)
$3\rightarrow 4$	137.0592	7.9(−4)
$3\rightarrow 5$	639.1326	3.8(−6)
$3\rightarrow 6$	1107.4482	1.4(−6)
$3\rightarrow 8$	1320.4789	2.8(−3)
$3\rightarrow 9$	1364.3699	3.6(−7)
$3\rightarrow 11$	1610.7538	4.0(−9)
$3\rightarrow 12$	1831.8771	3.8(−7)
$3\rightarrow 15$	2059.5095	1.3(−6)
$3\rightarrow 16$	2067.6368	6.9(−6)
$3\rightarrow 19$	2527.9914	1.4(−6)
$3\rightarrow 20$	2574.3849	1.2(−10)
$3\rightarrow 21$	2600.3037	1.8(−10)
$3\rightarrow 24$	2784.6144	1.9(−7)
$3\rightarrow 27$	3037.8863	4.8(−10)
$3\rightarrow 31$	3213.7305	1.6(−3)
$3\rightarrow 32$	3235.0080	1.0(−4)
$3\rightarrow 34$	3284.0013	1.5(−8)

Table 3. A sample of the $J=0\Rightarrow J=1$ parallel transitions having non-zero intensity. Columns are, from left to right: number of the vibrational states involved, calculated ro-vibrational energy difference, and calculated ro-vibrational band intensity $S_{\mathrm{Vib}}(V'', V')$. See Table 1 for full vibrational labels and levels. Powers of 10 are given in parenthesis.

Transition	ΔE cm^{-1}	Line str. (e Å)^2
$1\rightarrow 3$	1309.2493	7.4(−3)
$1\rightarrow 7$	2517.4545	1.2(−7)
$1\rightarrow 10$	2769.6759	1.4(−8)
$1\rightarrow 13$	3238.7180	2.6(−4)
$1\rightarrow 14$	3252.0056	4.9(−4)
$1\rightarrow 18$	3732.6711	4.1(−11)
$1\rightarrow 22$	3953.2825	3.1(−11)
$1\rightarrow 26$	4244.2485	2.5(−11)
$1\rightarrow 29$	4415.3899	9.3(−7)
$1\rightarrow 30$	4447.3147	2.8(−7)
$1\rightarrow 35$	4654.1652	2.8(−8)
$1\rightarrow 36$	4668.7921	2.3(−8)
$1\rightarrow 37$	4688.7381	1.4(−10)
$2\rightarrow 3$	709.3454	9.7(−7)
$2\rightarrow 7$	1917.2507	4.8(−7)
$2\rightarrow 10$	2169.7721	5.4(−12)
$2\rightarrow 13$	2638.8142	1.8(−7)
$2\rightarrow 14$	2652.1017	2.5(−7)
$2\rightarrow 18$	3132.7673	2.9(−10)
$2\rightarrow 23$	3397.4894	1.4(−11)
$2\rightarrow 29$	3815.4861	3.3(−7)
$2\rightarrow 30$	3845.0737	3.9(−8)
$2\rightarrow 35$	4054.2613	2.0(−10)
$2\rightarrow 36$	4068.8883	1.4(−10)
$3\rightarrow 4$	726.6849	1.2(−7)
$3\rightarrow 5$	1228.7556	3.9(−10)
$3\rightarrow 6$	1697.0739	1.7(−10)
$3\rightarrow 8$	1910.1047	4.1(−7)
$3\rightarrow 9$	1953.9959	5.5(−11)
$3\rightarrow 11$	2200.3793	2.1(−12)
$3\rightarrow 12$	2421.4991	1.8(−11)
$3\rightarrow 15$	2649.1365	2.7(−10)
$3\rightarrow 16$	2657.2566	9.0(−10)
$3\rightarrow 17$	2920.6113	3.3(−12)
$3\rightarrow 19$	3117.6169	1.5(−10)
$3\rightarrow 24$	3374.2397	1.9(−11)
$3\rightarrow 28$	3684.2893	3.0(−12)
$3\rightarrow 31$	3803.3624	1.7(−7)
$3\rightarrow 32$	3824.6494	1.2(−8)
$3\rightarrow 33$	3834.2869	4.0(−8)

Table 4. A sample of the fundamental state $J=0\Rightarrow J=1$ perpendicular transitions having non-zero intensity. Columns are, from left to right: number of the vibrational states involved, calculated ro-vibrational energy difference, and calculated ro-vibrational band intensity $S_{\mathrm{Vib}}(V'', V')$. See Table 1 for full vibrational labels and levels. Powers of 10 are given in parenthesis.

Transition	ΔE cm^{-1}	Line str. (e·Å)^2
$1\rightarrow 1$	602.2431	4.9(−4)
$1\rightarrow 2$	721.9615	6.7(−4)
$1\rightarrow 3$	1328.0506	2.0(−6)
$1\rightarrow 4$	1812.4478	6.5(−5)
$1\rightarrow 5$	1916.5797	3.0(−4)
$1\rightarrow 6$	1938.3300	6.3(−4)
$1\rightarrow 7$	2041.1770	2.7(−4)
$1\rightarrow 8$	2063.3524	2.7(−3)
$1\rightarrow 9$	2185.7748	9.6(−5)
$1\rightarrow 10$	2547.2766	6.3(−8)
$1\rightarrow 11$	2550.2981	2.0(−7)
$1\rightarrow 12$	2648.2523	1.3(−6)
$1\rightarrow 13$	2661.1525	6.6(−7)
$1\rightarrow 14$	2803.6048	3.0(−7)
$1\rightarrow 15$	3032.5222	1.5(−5)
$1\rightarrow 16$	3129.0022	3.3(−6)
$1\rightarrow 17$	3164.8115	7.4(−5)
$1\rightarrow 18$	3237.5819	7.5(−5)
$1\rightarrow 19$	3259.3201	5.6(−7)
$1\rightarrow 20$	3262.0690	2.0(−9)
$1\rightarrow 21$	3295.9179	1.5(−4)
$1\rightarrow 22$	3365.5350	6.9(−7)
$1\rightarrow 23$	3387.4716	2.6(−6)
$1\rightarrow 24$	3424.3011	1.6(−4)
$1\rightarrow 25$	3511.1900	1.3(−6)
$1\rightarrow 26$	3548.4275	7.9(−5)
$1\rightarrow 27$	3666.6381	1.8(−5)
$1\rightarrow 28$	3747.4305	4.2(−8)
$1\rightarrow 29$	3780.1826	2.9(−8)
$1\rightarrow 30$	3831.4614	2.9(−6)
$1\rightarrow 31$	3849.8935	1.1(−6)
$1\rightarrow 32$	3867.5780	2.3(−7)
$1\rightarrow 33$	3870.8252	3.8(−10)
$1\rightarrow 34$	3950.8765	5.2(−7)
$1\rightarrow 35$	3960.8140	6.7(−6)
$1\rightarrow 36$	3969.8855	2.0(−6)
$1\rightarrow 37$	3973.0352	1.0(−9)
$1\rightarrow 38$	3987.4937	2.9(−8)
$1\rightarrow 39$	4045.6299	1.3(−7)
$1\rightarrow 40$	4084.8814	3.5(−6)

parallel (and close) to the ideal one, showing that the DIPOLE4 code can efficiently scale up to at least some hundreds of processors. However full direct calculations are very expensive and were performed only up to $J=2$. The approximate line strength $S_{(f\leftarrow i)}=S_{\mathrm{Vib}}(V', V'')S_{\mathrm{Rot}}(J', J'')$ requires calculation of vibrational band intensities which are essentially integrals of the dipole function over all internal coordinates. This implies we only need to compute a matrix element of the form

$$\langle V'|\mu_\alpha|V''\rangle, \tag{19}$$

where $\alpha=x$, y, z and the z axis is conventionally chosen along the molecular symmetry axis. Since the basis functions (both FBR and DVR parts) are exactly the same as used in WAVR4 and DIPOLE4, DIPOLE4 was

Table 5. Comparison between our calculated individual ro-vibrational line position and intensities and experimental ones, for the $(3\nu_4 + \nu_5)$ combination band [34]. Columns, left to right, list: line type (branch and symmetry); J quantum number in the lower state; calculated frequency (cm^{-1}); experimental frequency (cm^{-1}); calculated S (cm $molecule^{-1}$); experimental S (cm $molecule^{-1}$); ratio between the calculated and experimental S. Powers of 10 are given in parenthesis.

Branch	J	E_{th}	E_{exp}	S_{th}	S_{exp}	S_{th}/S_{exp}
P_{ee}	1	2517.054	2558.242	1.47(−23)	1.29(−23)	1.14
P_{ee}	2	2514.633	2555.902	9.55(−24)	8.38(−24)	1.14
P_{ee}	3	2512.221	2553.576	4.14(−23)	3.77(−23)	1.10
P_{ee}	4	2509.816	2551.264	1.76(−23)	1.59(−23)	1.11
P_{ee}	5	2507.420	2548.967	6.20(−23)	5.55(−23)	1.12
P_{ee}	6	2505.032	2546.688	2.31(−23)	2.13(−23)	1.08
P_{ee}	7	2502.651	2544.426	7.43(−23)	6.69(−23)	1.11
P_{ee}	8	2500.278	2542.183	2.57(−23)	2.32(−23)	1.11
P_{ee}	9	2497.913	2539.962	7.80(−23)	6.95(−23)	1.12
P_{ee}	10	2495.556	2537.765	2.57(−23)	2.20(−23)	1.17
P_{ee}	11	2493.207	2535.592	7.43(−23)	6.53(−23)	1.14
P_{ee}	12	2490.865	2533.447	2.34(−23)	2.04(−23)	1.15
P_{ee}	14	2486.206	2529.241	1.98(−23)	1.69(−23)	1.17
P_{ee}	16	2481.579	2525.155	1.57(−23)	1.25(−23)	1.26
P_{ee}	17	2479.277	2523.158	4.09(−23)	3.23(−23)	1.27
P_{ee}	18	2476.983	2521.190	1.17(−23)	8.99(−24)	1.30
P_{ee}	19	2474.697	2519.251	2.95(−23)	2.28(−23)	1.29
P_{ee}	20	2472.419	2517.340	8.16(−24)	6.25(−24)	1.30
P_{ee}	21	2470.149	2515.458	2.00(−23)	1.47(−23)	1.36
R_{ee}	0	2521.918	2562.961	4.96(−24)	4.32(−24)	1.15
R_{ee}	1	2524.362	2565.342	2.95(−23)	2.60(−23)	1.14
R_{ee}	2	2526.814	2567.736	1.44(−23)	1.25(−23)	1.15
R_{ee}	3	2529.274	2570.146	5.56(−23)	4.96(−23)	1.12
R_{ee}	4	2531.742	2572.572	2.21(−23)	2.00(−23)	1.11
R_{ee}	5	2534.217	2575.015	7.52(−23)	6.64(−23)	1.13
R_{ee}	8	2541.692	2582.466	2.94(−23)	2.59(−23)	1.14
R_{ee}	10	2546.714	2587.553	2.88(−23)	2.41(−23)	1.20
R_{ee}	12	2551.768	2592.747	2.60(−23)	2.25(−23)	1.16
R_{ee}	14	2556.853	2598.059	2.19(−23)	1.79(−23)	1.22
R_{ee}	15	2559.408	2600.758	5.86(−23)	4.63(−23)	1.27
R_{ee}	16	2561.970	2603.485	1.72(−23)	1.31(−23)	1.31
R_{ee}	17	2564.541	2606.240	4.48(−23)	3.30(−23)	1.36
R_{ee}	18	2567.119	2609.022	1.28(−23)	9.09(−24)	1.41

also adapted to compute $\langle V'|\mu_\alpha|V''\rangle^2$. The integration over the FBR basis is carried out using quadrature similar to WAVR4 and the integration over the DVR basis is implemented simply as direct summation over the radial grids. Note however that WAVR4 does not use Eckart embedding and therefore the dipole components need to be transformed numerically. The transformation was implemented in a separate Fortran 90 module. For low-energy vibrational states of C_2H_2 the z axis of Eckart embedding is very nearly (but not exactly) coincident with the direction of the C–C bond, which in turn is conventionally chosen as the z axis of the diatom–diatom embedding we used for the WAVR4 calculations. It is therefore tempting to just perform the integral $\langle V'|\mu_z|V''\rangle$ with the μ_z component in this latter embedding. This is not strictly correct, as shown in detail by Le Sueur *et al.* [27], and we will indeed always consider the z component of the dipole moment in the Eckart embedding.

The wave functions of the ro-vibrational states with $J=1$ (the term ro-vibrational here is used in the sense of WAVR4 which makes no distinction between linear and non-linear molecules and treats them on equal footing) have vibrational angular momentum $l=1$ and, from these, we can also get transitions with $l=1$, $\Delta l=\pm 1$, i.e. perpendicular transitions.

6.1. *Results*

We used the DIPOLE4 code to compute ro-vibrational band intensities for all the pairs of states resulting from the run of WAVR4. Tables 2 to 4 report a sample of transitions having non-zero intensity. The states in Tables 2 to 4 are simply labelled by numbers in order

Table 6. Comparison between our calculated individual ro-vibrational line position and intensities and experimental ones, for the ν_3 fundamental band [36]. Columns, left to right, list: line type (branch and symmetry); J quantum number in the lower state; calculated line frequency (cm^{-1}); experimental frequency (cm^{-1}); calculated S (cm molecule^{-1}); experimental S (cm molecule^{-1}); ratio between the calculated and experimental S. Powers of 10 are given in parenthesis.

Branch	J	E_{th}	E_{exp}	S_{th}	S_{exp}	S_{th}/S_{exp}
P_e	2	3236.179	3290.125	3.89(−20)	2.61(−20)	1.49
P_e	3	3233.721	3287.754	1.69(−19)	1.13(−19)	1.50
P_e	6	3226.258	3280.592	9.40(−20)	6.30(−20)	1.49
P_e	7	3223.740	3278.187	3.03(−19)	2.05(−19)	1.48
P_e	8	3221.208	3275.774	1.05(−19)	7.02(−20)	1.50
P_e	9	3218.660	3273.351	3.18(−19)	2.14(−19)	1.49
P_e	10	3216.098	3270.918	1.05(−19)	7.17(−20)	1.46
P_e	11	3213.521	3268.477	3.03(−19)	2.08(−19)	1.46
P_e	12	3210.929	3266.025	9.55(−20)	6.50(−20)	1.47
P_e	13	3208.322	3263.563	2.66(−19)	1.84(−19)	1.45
P_e	14	3205.700	3261.090	8.09(−20)	5.55(−20)	1.46
P_e	15	3203.063	3258.607	2.18(−19)	1.52(−19)	1.43
P_e	16	3200.411	3256.112	6.40(−20)	4.39(−20)	1.46
P_e	17	3197.745	3253.606	1.67(−19)	1.16(−19)	1.44
P_e	18	3195.063	3251.087	4.76(−20)	3.28(−20)	1.45
P_e	19	3192.367	3248.556	1.20(−19)	8.48(−20)	1.42
P_e	20	3189.655	3246.011	3.33(−20)	2.31(−20)	1.44
P_e	21	3186.930	3243.454	8.18(−20)	5.68(−20)	1.44
P_e	22	3184.188	3240.882	2.29(−20)	1.56(−20)	1.47
R_e	1	3245.862	3299.521	1.20(−19)	7.76(−20)	1.55
R_e	3	3250.614	3304.167	2.26(−19)	1.46(−19)	1.55
R_e	4	3252.968	3306.476	8.99(−20)	5.81(−20)	1.55
R_e	5	3255.307	3308.776	3.05(−19)	1.94(−19)	1.57
R_e	6	3257.631	3311.067	1.11(−19)	6.98(−20)	1.59
R_e	7	3259.940	3313.349	3.50(−19)	2.18(−19)	1.61
R_e	8	3262.234	3315.620	1.19(−19)	7.43(−20)	1.60
R_e	9	3264.513	3317.881	3.58(−19)	2.24(−19)	1.60
R_e	10	3266.777	3320.131	1.17(−19)	7.30(−20)	1.60
R_e	11	3269.027	3322.370	3.36(−19)	2.14(−19)	1.57
R_e	13	3273.481	3326.812	2.92(−19)	1.79(−19)	1.63
R_e	14	3275.685	3329.016	8.85(−20)	5.46(−20)	1.62
R_e	15	3277.875	3331.205	2.38(−19)	1.45(−19)	1.64
R_e	17	3282.210	3335.545	1.81(−19)	1.09(−19)	1.66

of increasing energy. The complete list of calculated parallel and perpendicular ro-vibrational transitions is available on-line [58].

6.2. *Calculation of rotational constant B*

Since the available experimental data for parallel and perpendicular bands of C_2H_2 list positions and intensities of resolved ro-vibrational lines, we used the rigid rotor approximation, along with Hönl–London coefficients, to estimate the rotational structure for the transitions we computed. In this approximation, the energy difference between two ro-vibrational states is given by

$$\Delta E = \Delta E_{vib} + \Delta E_{rot}, \tag{20}$$

where ΔE_{vib} is tabulated in Table 1 and ΔE_{rot} is given by

$$\Delta E_{rot} = B_{v'}[J'(J'+1)] - B_{v''}[J''(J''+1)], \tag{21}$$

which results from the assumption of a rigid rotor and remembering $J=1$ ro-vibrational energy values that we calculated here. In Equation (21) $B_{v'}$ and $B_{v''}$ are the effective rotational constants in the upper and lower vibrational states involved in the transition, and J' and J'' are the quantum numbers of the total angular momentum in the upper and lower ro-vibrational states. Since we have both parallel and perpendicular transitions, ro-vibrational selection rules dictate that we can have $J'=J''+1$ (R branch), $J'=J''-1$ (P branch) and $J'=J'$ (Q branch). The effective rotational constant B_v value for each vibrational state is calculated as the difference $\Delta E - \Delta E_{vib}$.

Table 7. Comparison between our calculated individual ro-vibrational line position and intensities and experimental ones, for the ν_5 fundamental band [37]. Columns, left to right, list: line type (branch); J quantum number in the lower state; calculated line frequency (cm^{-1}); experimental frequency (cm^{-1}); calculated S(cm molecule^{-1}); experimental S (cm molecule^{-1}); ratio between the calculated and experimental S. Powers of 10 are given in parenthesis.

Branch	J	E_{th}	E_{exp}	S_{th}	S_{exp}	S_{th}/S_{exp}
P_{ee}	14	687.095	687.818	1.79(−20)	1.50(−20)	1.19
P_{ee}	13	689.640	690.065	6.57(−21)	5.38(−21)	1.22
P_{ee}	12	692.176	692.318	2.13(−20)	1.76(−20)	1.21
P_{ee}	11	694.704	694.577	7.53(−21)	6.10(−21)	1.23
P_{ee}	10	697.223	696.843	2.35(−20)	1.89(−20)	1.24
P_{ee}	8	702.237	701.397	2.37(−20)	1.86(−20)	1.27
P_{ee}	6	707.218	705.983	2.14(−20)	1.74(−20)	1.23
P_{ee}	5	709.696	708.289	6.41(−21)	5.29(−21)	1.21
P_{ee}	4	712.166	710.604	1.64(−20)	1.33(−20)	1.23
P_{ee}	3	714.627	712.928	4.31(−21)	3.78(−21)	1.14
P_{ee}	2	717.080	715.262	8.97(−21)	8.58(−21)	1.05
P_{ee}	1	719.525	717.606	1.54(−21)	1.96(−21)	0.79
Q_{ef}	23	719.670	719.282	4.17(−21)	3.06(−21)	1.36
Q_{ef}	21	720.044	719.479	6.51(−21)	5.06(−21)	1.29
Q_{ef}	20	720.219	719.561	2.65(−21)	2.10(−21)	1.26
Q_{ef}	19	720.385	719.633	9.60(−21)	8.06(−21)	1.19
Q_{ef}	18	720.542	719.695	3.80(−21)	3.28(−21)	1.16
Q_{ef}	17	720.692	719.748	1.34(−20)	1.29(−20)	1.04
Q_{ef}	16	720.833	719.793	5.14(−21)	4.85(−21)	1.06
Q_{ef}	14	721.090	719.861	6.52(−21)	6.41(−21)	1.02
Q_{ef}	13	721.206	719.887	2.15(−20)	2.24(−20)	0.96
Q_{ef}	12	721.314	719.907	7.74(−21)	8.09(−21)	0.96
Q_{ef}	11	721.414	719.922	2.46(−20)	2.67(−20)	0.92
Q_{ef}	10	721.505	719.934	8.54(−21)	9.42(−21)	0.91
R_{ee}	1	726.810	724.693	1.06(−21)	9.66(−22)	1.09
R_{ee}	2	729.221	727.073	6.37(−21)	5.71(−21)	1.12
R_{ee}	4	734.020	731.862	1.28(−20)	1.12(−20)	1.14
R_{ee}	5	736.406	734.269	5.22(−21)	4.46(−21)	1.17
R_{ee}	6	738.785	736.684	1.79(−20)	1.52(−20)	1.18
R_{ee}	7	741.155	739.107	6.23(−21)	5.53(−21)	1.13
R_{ee}	8	743.517	741.537	2.14(−20)	1.82(−20)	1.18
R_{ee}	9	745.870	743.973	7.09(−21)	6.04(−21)	1.17
R_{ee}	10	748.215	746.415	2.19(−20)	1.81(−20)	1.21
R_{ee}	11	750.552	748.862	7.51(−21)	6.19(−21)	1.21
R_{ee}	12	752.881	751.313	2.13(−20)	1.75(−20)	1.22
R_{ee}	13	755.201	753.769	6.99(−21)	5.66(−21)	1.24

7. Calculations of line intensities

In this section we will compare the results of our calculations with available experimental data, taken from publications referred to by HITRAN [34,36–38]. Such experimental data come in the form of lists of resolved ro-vibrational lines, each with its position and integrated line strength. Since our present variational calculations were restricted to the total angular momentum $J=1$, we estimated the rotational substructure in the rigid rotor approximation. The integrated line strength of a given transition is given by [62]

$$S(T_0) = \left(\frac{2\pi^2}{3hc\epsilon_0}\right)\left[\frac{g''\tilde{\nu}_0}{g_V Q(T_0)}\right] S_{vib} L(J,l) \exp\left(\frac{-E''}{kT_0}\right) \times \left[1-\exp\left(\frac{-hc\tilde{\nu}_0}{kT_0}\right)\right], \quad (22)$$

where: g'' is the statistical weight due to nuclear spin of the lower level (1 for para and 3 for ortho states); $\tilde{\nu}_0$ is the transition wavenumber; g_V is a factor used to consider bands with l-type doubling (g_V is equal to 2 in such a case, otherwise, it is equal to 1); $Q(T_0)$ is the total partition function at temperature T_0, we used $Q(T_0)=405.867$ [37]; $L(J,l)$ is the Hönl–London factor, J being the rotational quantum number of the lower level of the transition, and l its total vibrational quantum number ($l=|l_4+l_5|$); E'' is the energy of the lower level.

Equation (22) is used in HITRAN to *derive*, in a multi-spectrum fit procedure [63], the value of S_{vib}. In that procedure, S_{vib} is actually considered itself a (slowly varying) function of J, and fitted with a second-order polynomial in J with the so-called

Herman–Wallis coefficients [30]. The apparent variability of S_{vib} accounts for the interaction between vibrational and angular motions, which is not explicitly considered in Equation (22). In a full variational calculation (i.e. one *including* states with $J>1$) one does not assume the line intensity to be factorised as, with $S_{\mathrm{Rot}}(J'',J')=L(J,l)$, but directly computes the value of S. However, we use Equation (22) to compare our results with the lists of ro-vibrational transitions in HITRAN. Since our current calculation does not include the Herman–Wallis coefficients, we expect our calculated line intensities to be most accurate for low J values, for which separation between rotational and vibrational motion is a better approximation. Below we show a detailed comparison for three bands. The $(3\nu_4+\nu_5)$ combination band has a calculated origin at $2519.5\,\mathrm{cm}^{-1}$, versus a measured value of $2560.6\,\mathrm{cm}^{-1}$. Our calculated value of S_{vib} is $1.6\times10^{-6}\,\mathrm{D}^2$, versus an experimental value (derived from multi-spectrum fit) of $1.7\times10^{-6}\,\mathrm{D}^2$. Table 5 reports a line by line comparison with the results of paper [34]. The ν_3 fundamental band has a calculated origin at $3241.1\,\mathrm{cm}^{-1}$, versus a measured value of $3316.9\,\mathrm{cm}^{-1}$. Our calculated value of S_{vib} is $5.1\times10^{-3}\,\mathrm{D}^2$, versus an experimental value (derived from multi-spectrum fit) of $3.9\times10^{-3}\,\mathrm{D}^2$. Table 6 reports a line by line comparison with the results of paper [36]. The ν_5 fundamental band has a calculated origin at $722.2\,\mathrm{cm}^{-1}$, versus a measured value of $730.3\,\mathrm{cm}^{-1}$. Our calculated value of S_{vib} is $5.8\times10^{-2}\,\mathrm{D}^2$, versus an experimental value (derived from multi-spectrum fit) of $9.8\cdot10^{-2}\,\mathrm{D}^2$. Table 7 reports a line by line comparison with the results of the paper [37].

8. Conclusions and perspectives

Our aim is to develop a general procedure for calculating spectra of hot molecules of astrophysical interest. The acetylene molecule provides the initial application. It is worth considering the steps required to achieve this aim. Our *ab initio* calculated energies differ from the experimental ones by up to about $100\,\mathrm{cm}^{-1}$, which cannot be considered a good level of agreement and it is clear that more work in this area is needed before we can produce a final line list. Better transition energies can be obtained by semi-empirical methods. One strategy is to tune the *ab initio* potential energy surface using spectroscopic data [47]; an alternative approach is to substitute the calculated energy levels with measured ones [64]. In practise a combination of both approaches has proved successful [65].

The results of the DIPOLE4 code and our new dipole surface have been compared with the HITRAN database, using an approximation that speeds up the test calculations by more than one order of magnitude. This resulted in its successful validation, since calculated values were compatible with experimental data. The discrepancies can be accounted for by the simplifying assumptions adopted in the calculations and, possibly, by the rather low-level *ab initio* method used to calculate the dipole moment surface. However, the tests presented in Section 4 suggest this dipole moment surface actually performs better than what it could be expected from the level of theory employed. Experience has shown that such dipole moment surfaces are best calculated *ab initio* [66] and this can lead to predicted intensities competitive in accuracy with laboratory measurements [67,68]. It may also be necessary to relax such simplifications used in the nuclear motion calculations: moving the variational calculations one step further by fully including in it the rotational degrees of freedom. This will enable us to obtain complete lists of vibrational energy levels up to a given maximum excitation (i.e. including all states with non-zero vibrational angular momentum) and consequently of the electric dipole transitions among them which are allowed, including those perpendicular bands, such as transitions involving Δ states, which we have not considered here.

A complete line list of transitions will enable us to estimate the opacity of C_2H_2 at the temperatures prevailing in the photospheres of cool stars (i.e. between 1000 and 2000 K). Such lists of states and transitions will be suitable for straightforward integration in existing models of stellar atmospheres, to estimate their effect on radiation transport, their physical structure and the resulting spectra. One will also be able to use the molecular data as they are, to directly estimate C_2H_2 absorption spectra at a given temperature, for straight comparison with available observational data.

Acknowledgements

We would like to thank E. Mátyus for kindly providing the program routine calculating the Eckart embedding. We also thank H. Dhanoa for helpful discussion and CCP6 (the Collaborative Computational Project on Molecular Quantum Dynamics) for support. The work of B.J.B. was supported by the U.S. Department of Energy under contract no. DE-FG02-07ER54914. One of the authors (A.U.) would like to thank Dr Lorenzo Lodi for his useful suggestions and R.A.S. program PO Sardegna FSE 2007-2013 L.R. 7/2007 'Promozione della ricerca scientifica e dell'innovazione tecnologica in Sardegna' for funding his work.

References

[1] S. Wylie Miller, *Oxy-Acetylene Welding* (Gadow Press, 2008).
[2] P.F. Coheur, P.F. Bernath, M. Carleer, R. Colin, O.L. Polyansky, N.F. Zobov, R.J.B.S.V. Shirin and J. Tennyson, J. Chem. Phys. **122**, 074307 (2005).
[3] S.T. Ridgway, Astrophys. J. Lett. **187**, L41 (1974).
[4] M. Combes, T. Encrenaz, L. Vapillon, Y. Zeau and C. Lesqueren, Astron. Astrophys. **34**, 33 (1974).
[5] T. Encrenaz, H. Feuchtgruber, S.K. Atreya, B. Bezard, E. Lellouch, J. Bishop, S. Edgington, T. Degraauw, M. Griffin and M.F. Kessler, Astron. Astrophys. **333**, L43 (1998).
[6] A. Goldman, F.J. Murcray, R.D. Blatherwick, J.R. Gillis, F.S. Bonomo, F.H. Murcray, D.G. Murcray and R.J. Cicerone, J. Geophys. Res. **86**, 12143 (1981).
[7] C.P. Rinsland, A. Baldacci and K.N. Rao, Astrophys. J. Suppl. Ser. **49**, 487 (1982).
[8] J.J. Hillman, D.E. Jennings, G.W. Halsey, S. Nadler and W.E. Blass, J. Mol. Spectrosc. **146**, 389 (1991).
[9] J. Cernicharo, I. Yamamura, E. González-Alfonso, T. de Jong, A. Heras, R. Escribano and J. Ortigoso, Astrophys. J. Lett. **526**, L41 (1999).
[10] W. Aoki, T. Tsuji and K. Ohnaka, Astron. Astrophys. **350**, 945 (1999).
[11] G.J. Harris, Y.V. Pavlenko, H.R.A. Jones and J. Tennyson, Mon. Not. Roy. Astron. Soc. **344**, 1107 (2003).
[12] R. Loidl, A. Lançon and U.G. Jørgensen, Astron. Astrophys. **371**, 1065 (2001).
[13] J. Tennyson, G.J. Harris, R.J. Barber, S. La Delfa, B.A. Voronin, B.M. Kaminsky and Y.V. Pavlenko, Mol. Phys. **105**, 701 (2007).
[14] S.N. Yurchenko, R.J. Barber, A. Yachmenev, W. Theil, P. Jensen and J. Tennyson, J. Phys. Chem. A **113**, 11845 (2009).
[15] R. Warmbier, R. Schneider, B.J. Braams, J.M. Bowman and P.H. Hauschildt, Astron. Astrophys. **495**, 655 (2009).
[16] J. Bowman, S. Carter and H. Huang, Int. Rev. Phys. Chem. **22**, 533 (2003).
[17] M.J. Bramley and N.C. Handy, J. Chem. Phys. **98**, 1378 (1993).
[18] J.M.L. Martin, T.J. Lee and P.R. Taylor, J. Chem. Phys. **108**, 676 (1998).
[19] S. Carter and N.C. Handy, Mol. Phys. **100**, 681 (2002).
[20] M. Herman, J. Liévin, J. Vander Auwera and A. Campargue, *Global and Accurate Vibration Hamiltonians from High-resolution Molecular Seectrodcopy, in series. Advances in Chemical Physics*, Vol. 108 (Wiley, New York, 1999).
[21] M.P. Jacobson and R.W. Field, J. Phys. Chem. **104**, 3073 (2000).
[22] I.N. Kozin, M.M. Law, J. Tennyson and J.M. Hutson, Comput. Phys. Commun. **163**, 117 (2004).
[23] I.N. Kozin, M.M. Law, J. Tennyson and J.M. Hutson, J. Chem. Phys. **122** (6), 064309 (2005).
[24] M. Abbouti Temsamani, J.M. Champion and S. Oss, J. Chem. Phys. **110**, 2893 (1999).
[25] P.R. Bunker and P. Jensen, *Molecular Symmetry and Spectroscopy*, 2nd ed. (NRC Research, Ottawa, 1998).
[26] R.N. Zare, *Angular Momentum: Understanding Spatial Aspects in Chemistry and Physics*, 1st ed. (Wiley-Interscience, New York, 1988).
[27] C.R. Le Sueur, S. Miller, J. Tennyson and B.T. Sutcliffe, Mol. Phys. **76**, 1147 (1992).
[28] C. Eckart, Phys. Rev. **47**, 552 (1935).
[29] H. Hönl and F. London, Naturwissenschaften **13**, 756 (1925).
[30] P.F. Bernath, *Spectra of Atoms and Molecules* (Oxford University Press, Oxford, 2005).
[31] L.S. Rothman, R.R. Gamache, A. Goldman, L.R. Brown, R.A. Toth, H.M. Pickett, R.L. Poynter, J.M. Flaud, C. Camy-Peyret, A. Barbe, N. Husson, C.P. Rinsland and M.A.H. Smith, Appl. Opt. **26**, 4058 (1987).
[32] L.S. Rothman, D. Jacquemart, A. Barbe, D. Chris Benner, M. Birk, L.R. Brown, M.R. Carleer, C. Chackerian, K. Chance, L.H. Coudert, V. Dana, V.M. Devi, J.M. Flaud, R.R. Gamache, A. Goldman, J.M. Hartmann, K.W. Jucks, A.G. Maki, J.Y. Mandin, S.T. Massie, J. Orphal, A. Perrin, C.P. Rinsland, M.A.H. Smith, J. Tennyson, R.N. Tolchenov, R.A. Toth, J. Vander Auwera, P. Varanasi and G. Wagner, J. Quantum Spectrosc. Radiat. Transf. **96**, 139 (2005).
[33] L.S. Rothman, I.E. Gordon, A. Barbe, D. Chris Benner, P.B. Bernath, M. Birk, V. Boudon, L.R. Brown, A. Campargue, J.P. Champion, K. Chance, L.H. Coudert, V. Dana, V.M. Devi, S. Fally, J.M. Flaud, R.R. Gamache, A. Goldman, D. Jacquemart, I. Kleiner, N. Lacome, J.M. Lafferty, J.Y. Mandin, S.T. Massie, S.N. Mikhailenko, C.E. Miller, N. Moazzen-Ahmadi, O.V. Naumenko, A.V. Nikitin, J. Orphal, V.I. Peralov, A. Perrin, A. Predoi-Cross, C.P. Rinsland, M. Rotger, M. Simeckova, M.A.H. Smith, K. Sung, S.A. Tashkun, J. Tennyson, R.A. Toth, A.C. Vandaele and J. Vander Auwera, J. Quantum Spectrosc. Radiat. Transf. **110**, 533 (2009).
[34] D. Jacquemart, N. Lacome, J.Y. Mandin, V. Dana, O.M. Lyulin and V.I. Perevalov, J. Quantum Spectrosc. Radiat. Transf. **103**, 478 (2007).
[35] D. Jacquemart, J.Y. Mandin, V. Dana, C. Claveau, J. Vander Auwera, M. Herman, L.S. Rothman, L. Regalia-Jarlot and A. Barbe, J. Quantum Spectrosc. Radiat. Transf. **82**, 363 (2003).
[36] J.Y. Mandin, D. Jacquemart, V. Dana, L. Regalia-Jarlot and A. Barbe, J. Quantum Spectrosc. Radiat. Transf. **92**, 239 (2005).
[37] D. Jacquemart, C. Claveau, J.Y. Mandin and V. Dana, J. Quantum Spectrosc. Radiat. Transf. **67**, 429 (2000).
[38] J.Y. Mandin, V. Dana and C. Claveau, J. Quantum Spectrosc. Radiat. Transf. **69**, 81 (2001).
[39] P. Varanasi, L.P. Giver and F.P.J. Valero, J. Quantum Spectrosc. Radiat. Transf. **30**, 497 (1983).

[40] O.M. Lyulin, V.I. Perevalov, J.Y. Mandin, V. Dana, F. Gueye, X. Thomas, P. von der Heyden, D. Décatoire, L. Régalia-Jarlot, D. Jacquemart and N. Lacome, J. Quantum Spectrosc. Radiat. Transf. **103**, 496 (2007).
[41] O.M. Lyulin, D. Jacquemart, N. Lacome, V.I. Perevalov and J.Y. Mandin, J. Quantum Spectrosc. Radiat. Transf. **109**, 1856 (2008).
[42] S. Carter and I.M. Mills, Mol. Phys. **41**, 191 (1980).
[43] L. Halonen, M.S. Child and S. Carter, Mol. Phys. **47**, 1097 (1982).
[44] C.E. Dykstra and H.F. Schaefer III, J. Am. Chem. Soc. **100**, 1378 (1978).
[45] S. Zou, J.M. Bowman and A. Brown, J. Chem. Phys. **118**, 10012 (2003).
[46] S. Zou and J.M. Bowman, J. Chem. Phys. **117**, 5507 (2002).
[47] S. Zou and J.M. Bowman, Chem. Phys. Lett. **368**, 421 (2003).
[48] D. Xu, H. Guo, S. Zou and J.M. Bowman, Chem. Phys. Lett. **377**, 582 (2003).
[49] A.D. Boese, N.L. Doltsinis, N.C. Handy and M. Sprik, J. Chem. Phys. **112**, 1670 (2000).
[50] T.H. Dunning Jr., J. Chem. Phys. **90**, 1007 (1989).
[51] H.-J Werner, P.J. Knowles, R. Lindh, F.R. Manby, M. Schz, P. Celani, T. Korona, A. Mitrushenkov, G. Rauhut, T.B. Adler, R.D. Amos, A. Bernhardsson, A. Berning, D.L. Cooper, M.J.O. Deegan, A.J. Dobbyn, F. Eckert, E. Goll, C. Hampel, G. Hetzer, T. Hrenar, G. Knizia, C. Kpl, Y. Liu, A.W. Lloyd, R.A. Mata, A.J. May, S.J. McNicholas, W. Meyer, M.E. Mura, A. Nickla P. Palmieri, K. Pfler, R. Pitzer, M. Reiher, U. Schumann, H. Stoll, A.J. Stone, R. Tarroni, T. Thorsteinsson, M. Wang, A. Wolf, MOLPRO, version 2006.1, a package of *ab initio* programs 2008, see www.molpro.net.
[52] X.C. Huang, B.J. Braams and J.M. Bowman, J. Chem. Phys. **112**, 044308 (2005).
[53] H. Derksen and G. Kemper, *Computational Invariant Theory* (Springer Verlag, Berlin, 2002).
[54] W. Bosma, J. Cannon and C. Playoust, J. Symb. Comp. **24**, 235 (1997).
[55] B.J. Braams and J.M. Bowman, Int. Rec Phys. Chem. **28** (4), 577, http://magma.maths.usyd.edu.au/magma/ (2009).
[56] J. Tennyson, J.R. Henderson and N.G. Fulton, Comput. Phys. Commun. **86**, 175 (1995).
[57] J. Tennyson and B.T. Sutcliffe, J. Chem. Phys. **77**, 4061 (1982).
[58] Supplementary material can be retrieved from http://astrochemistry.dsf.unica.it/~aurru/.
[59] M. Herman, A. Campargue, M.I. El Idrissi and J. Vander Auwera, J. Phys. Chem. Ref. Data **32**, 921 (2003).
[60] M.P. Jacobson, R.J. Silbey and R.W. Field, J. Chem. Phys. **110**, 845 (1999).
[61] J. Tennyson, M.A. Kostin, P. Barletta, G.J. Harris, O.L. Polyansky, J. Ramanlal and N.F. Zobov, Comput. Phys. Comm. **163**, 85 (2004).
[62] O.M. Lyulin, V.I. Perevalov, J.Y. Mandin, V. Dana, D. Jacquemart, L. Régalia-Jarlot and A. Barbe, J. Quantum Spectrosc. Radiat. Transf. **97**, 81 (2006).
[63] D. Jacquemart, J.Y. Mandin, V. Dana, N. Picqué and G. Guelachvili, Eur. Phys. J. D **14**, 55 (2001).
[64] G.J. Harris, J. Tennyson, B.M. Kaminsky, Y.V. Pavlenko and H.R.A. Jones, Mon. Not. R. astr. Soc. **367**, 400 (2006).
[65] R.J. Barber, J. Tennyson, G.J. Harris and R.N. Tolchenov, Mon. Not. R. Astr. Soc. **368**, 1087 (2006).
[66] A.E. Lynas-Gray, S. Miller and J. Tennyson, J. Mol. Spectrosc. **169**, 458 (1995).
[67] L. Lodi, R.N. Tolchenov, J. Tennyson, A.E. Lynas-Gray, S.V. Shirin, N.F. Zobov, O.L. Polyansky, A.G. Császár, J. Tennyson, J. van Stralen and L. Visscher, J. Chem. Phys. **128**, 044304 (2008).
[68] L. Lodi and J. Tennyson, J. Quantum Spectrosc. Rad. Transf. **109**, 1219 (2008).
[69] M. Mladenović, J. Chem. Phys. **112**, 1070 (2000).

Appendix 1

Following Bunker and Jensen [25] [Equation (14–6)], let us assume that the component of the molecular dipole moment operator along the A-axis is given by

$$\mu_A = \sum_j e_j R_j, \tag{23}$$

where e_j and R_j are the charge and coordinates of the jth particle in the molecule, and j runs over all nuclei and electrons; $A = X$, Y, or Z and (X, Y, Z) is a coordinate system space fixed at the nuclear centre of mass. Then the line strength for a neutral molecule is

$$S_{(f\leftarrow i)} = \sum_{\Phi'\Phi} \sum_{A=X,Y,Z} |\langle \Phi' | \mu_A | \Phi \rangle|^2, \tag{24}$$

where the first sum runs over all (degenerate) eigenfunctions Φ' and Φ with energies E' and E respectively. In practise, ro-vibrational eigenfunctions are obtained in the molecule-fixed axis system and therefore we need to transform the dipole moment operators into the molecule-fixed coordinate system. This can be compactly given by Bunker and Jensen [25] [Equation (14–15)]

$$\mu_s^{(1,\sigma)} = \sum_{\sigma''=-1}^{1} \left[D^{(1)}_{\sigma\sigma''}(\phi, \theta, \chi) \right]^* \mu_m^{(1,\sigma'')}, \tag{25}$$

where the space fixed components of the dipole moment are given by

$$\mu_s^{(1,\pm 1)} = [\mp \mu_X - \mathrm{i}\mu_Y]/2^{1/2}, \tag{26}$$

$$\mu_s^{(1,0)} = \mu_Z \tag{27}$$

and similarly the molecule fixed components are

$$\mu_m^{(1,\pm 1)} = [\mp \mu_x - \mathrm{i}\mu_y]/2^{1/2}, \tag{28}$$

$$\mu_m^{(1,0)} = \mu_z. \tag{29}$$

Then the line strength equation above becomes

$$S_{(f\leftarrow i)} = \sum_{\Phi'\Phi}\sum_{\sigma=-1}^{1} |\langle\Phi'|\mu_s^{(1,\sigma)}|\Phi\rangle|^2 = \sum_{\Phi'\Phi}\sum_{\sigma=-1}^{1}\left|\sum_{\sigma''=-1}^{1}\langle\Phi'|D^{(1)*}_{\sigma\sigma''}\mu_m^{(1,\sigma'')}|\Phi\rangle\right|^2. \quad (30)$$

The basis functions used by WAVR4 [22] are a direct product of radial and angular functions. The angular functions are non-direct product and include symmetric top functions. Thus the eigenfunctions obtained in the process of Hamiltonian diagonalisation are linear combinations of basis functions

$$|\Phi\rangle = \sum_{i,i_1,i_2,i_3} a_{i,i_1,i_2,i_3}|i\rangle|i_1\rangle|i_2\rangle|i_3\rangle, \quad (31)$$

where $|i_1\rangle$, $|i_2\rangle$ and $|i_3\rangle$ are radial basis functions (they are essentially radial grid points) and the angular function is given by

$$|i\rangle = N_{Kk}\kappa^k P_j^{|k-\kappa K|}\left[Y_l^{\kappa k}|J,K,M\rangle + (-1)^{J+p+K+k}Y_l^{-\kappa k}|J,-K,M\rangle\right]. \quad (32)$$

In the last equation, N_{Kk} is the normalisation coefficient $1/[2(1+\delta_{K0}\delta_{k0})]^{1/2}$, κ is an auxiliary (quantum) number taking values $+1$ or -1, p is the parity quantum number taking values 0 or 1, j, l and k are angular momentum quantum numbers, and $|J,K,M\rangle$ is a symmetric top wave function. Note that i is assumed to be an aggregate quantum number running over all possible combinations of j, l, k, κ, K, and M (p and J are strict quantum numbers and therefore are the same for the whole eigenfunction). Then the expectation value of a dipole operator is given by

$$\langle\Phi'|D^{(1)*}_{\sigma\sigma''}\mu_m^{(1,\sigma'')}|\Phi\rangle = \sum_{i,i'}\sum_{i_1,i_2,i_3} a_{i',i'_1,i'_2,i'_3}\, a_{i,i_1,i_2,i_3}\langle i'|D^{(1)*}_{\sigma\sigma''}\mu_m^{(1,\sigma'')}|i\rangle, \quad (33)$$

where we used an approximation that $\langle i'_1|\langle i'_2|\langle i'_3|\mu_m^{(1,\sigma'')}|i_1\rangle|i_2\rangle|i_3\rangle = \mu_m^{(1,\sigma'')}\delta_{i_1i'_1}\delta_{i_2i'_2}\delta_{i_3i'_3}$. That is we used the diagonal approximation for the dipole moment function in the grid basis. It means the integration over the radial basis is reduced to taking the values of the dipole function at the grid points. After substituting the expression for $|i\rangle$ we obtain

$$\begin{aligned}\langle\Phi'|D^{(1)*}_{\sigma\sigma''}\mu_m^{(1,\sigma'')}|\Phi\rangle &= \sum_{i,i'}\sum_{i_1,i_2,i_3} a_{i',i'_1,i'_2,i'_3}\, a_{i,i_1,i_2,i_3} N_{K'k'}(\kappa')^{k'}N_{Kk}(\kappa)^k \iint \mathrm{d}\Omega P_{j'}^{|k'-\kappa'K'|} \\ &\times P_j^{|k-\kappa K|}\Big[Y_{l'}^{*\kappa'k'}\mu_m^{(1,\sigma'')}Y_l^{\kappa k}\langle J',K',M'|D^{(1)*}_{\sigma\sigma''}|J,K,M\rangle \\ &+(-1)^{J'+p'+K'+k'}\,Y_{l'}^{*-\kappa'k'}\mu_m^{(1,\sigma'')}Y_l^{\kappa k}\langle J',-K',M'|D^{(1)*}_{\sigma\sigma''}|J,K,M\rangle \\ &+(-1)^{J+p+K+k}\,Y_{l'}^{*\kappa'k'}\mu_m^{(1,\sigma'')}Y_l^{-\kappa k}\langle J',K',M'|D^{(1)*}_{\sigma\sigma''}|J,-K,M\rangle \\ &+(-1)^{J'+p'+K'+k'+J+p+K+k}\,Y_{l'}^{*-\kappa'k'}\mu_m^{(1,\sigma'')}Y_l^{-\kappa k} \\ &\times\langle J',-K',M'|D^{(1)*}_{\sigma\sigma''}|J,-K,M\rangle\Big], \end{aligned} \quad (34)$$

where $\mu_m^{(1,\sigma'')}$ is assumed to depend only on the internal angular coordinates and the radial coordinates take the values of the radial grid points.

Integrating over the Euler angles (Equation (14-23) [25]), the expression in square brackets above becomes

$$\begin{aligned}[\ldots] &= (-1)^{M'}[(2J+1)(2J'+1)]^{1/2}\begin{pmatrix}J & 1 & J'\\ M & \sigma & -M'\end{pmatrix} \\ &\times\left\{Y_{l'}^{*\kappa'k'}\mu_m^{(1,\sigma'')}Y_l^{\kappa k}\begin{pmatrix}J & 1 & J'\\ K & \sigma'' & -K'\end{pmatrix}(-1)^{K'}\right. \\ &+Y_{l'}^{*-\kappa'k'}\mu_m^{(1,\sigma'')}Y_l^{\kappa k}\begin{pmatrix}J & 1 & J'\\ K & \sigma'' & K'\end{pmatrix}(-1)^{J'+p'+K'+k'}(-1)^{-K'} \\ &+Y_{l'}^{*\kappa\kappa'k'}\mu_m^{(1,\sigma'')}Y_l^{-\kappa k}\begin{pmatrix}J & 1 & J'\\ -K & \sigma'' & -K'\end{pmatrix}(-1)^{J+p+K+k}(-1)^{K'} \\ &+Y_{l'}^{*-\kappa'k'}\mu_m^{(1,\sigma'')}Y_l^{-\kappa k}\begin{pmatrix}J & 1 & J'\\ -K & \sigma'' & K'\end{pmatrix} \\ &\times(-1)^{J'+p'+K'+k'+J+p+K+k}(-1)^{-K'}\Big\}. \end{aligned} \quad (35)$$

Clearly if a is an integer then $(-1)^a = (-1)^{-a}$. Since K in our case is an integer $(-1)^{K'} = (-1)^{-K'}$ and therefore $(-1)^{K'}$ can be taken away as a common factor.

Our spherical harmonics are defined as in Equation (31) of Mladenović [69]. Since κ is equal to -1 or 1 and k is not negative, the expectation value of the dipole moment function is

$$\begin{aligned}&\langle\Phi'|\mu_s^{(1,\sigma)}|\Phi\rangle \\ &= \sum_{i',i,i_1,i_2,i_3} a_{i',i_1,i_2,i_3}a_{i,i_1,i_2,i_3}N_{K'k'}(\kappa')^{k'}N_{Kk}(\kappa)^k \\ &\times\iint \mathrm{d}\Omega\, P_{j'}^{|k'-\kappa'K'|}P_j^{|k-\kappa K|}(-1)^{M'+K'}[(2J+1)(2J'+1)]^{1/2} \\ &\times\begin{pmatrix}J & 1 & J'\\ M & \sigma & -M'\end{pmatrix}\sum_{\sigma''=-1}^{1}\mu_m^{(1,\sigma'')} \\ &\times\frac{1}{2\pi}\Big[P_{l'}^{k'}P_l^k\, e^{i(-\kappa'k'+\kappa k)\chi}\begin{pmatrix}J & 1 & J'\\ K & \sigma'' & -K'\end{pmatrix}(-1)^{\frac{-\kappa'+1}{2}k'+\kappa'k'+\frac{\kappa+1}{2}k} \\ &+P_{l'}^{k'}P_l^k\exp[\mathrm{i}(\kappa'k'+\kappa k)\chi]\begin{pmatrix}J & 1 & J'\\ K & \sigma'' & K'\end{pmatrix} \\ &\times(-1)^{\frac{\kappa'+1}{2}k'+\kappa'k'+\frac{\kappa+1}{2}k+J'+p'+K'+k'} \\ &+P_{l'}^{k'}P_l^k\exp[\mathrm{i}(-\kappa'k'-\kappa k)\chi]\begin{pmatrix}J & 1 & J'\\ -K & \sigma'' & -K'\end{pmatrix} \\ &\times(-1)^{\frac{-\kappa'+1}{2}k'+\kappa'k'+\frac{-\kappa+1}{2}k+J+p+K+k} \\ &+P_{l'}^{k'}P_l^k\exp[\mathrm{i}(\kappa'k'-\kappa k)\chi]\begin{pmatrix}J & 1 & J'\\ -K & \sigma'' & K'\end{pmatrix} \\ &\times(-1)^{\frac{\kappa'+1}{2}k'+\kappa'k'+\frac{-\kappa+1}{2}k+J'+p'+K'+k'+J+p+K+k}\Big]. \end{aligned} \quad (36)$$

Removing the obvious common factors and simplifying the result we obtain

$$\begin{aligned}&\langle\Phi'|\mu_s^{(1,\sigma)}|\Phi\rangle \\ &= (-1)^{M'}[(2J+1)(2J'+1)]^{1/2}\begin{pmatrix}J & 1 & J'\\ M & \sigma & -M'\end{pmatrix} \\ &\times\sum_{i',i,i_1,i_2,i_3} a_{i',i_1,i_2,i_3}a_{i,i_1,i_2,i_3}N_{K'k'}(\kappa')^{k'}N_{Kk}(\kappa)^k(-1)^{K'} \\ &\times\iint \mathrm{d}\Omega\, P_{j'}^{|k'-\kappa'K'|}P_j^{|k-\kappa K|}P_{l'}^{k'}P_l^k\frac{1}{2\pi}\sum_{\sigma''=-1}^{1}\mu_m^{(1,\sigma'')} \end{aligned}$$

$$\times\left[\exp[\mathrm{i}(-\kappa' k'+\kappa k)\chi]\begin{pmatrix} J & 1 & J' \\ K & \sigma'' & -K'\end{pmatrix}(-1)^{\frac{\kappa'+1}{2}k'+\frac{\kappa+1}{2}k}\right.$$
$$+\exp[\mathrm{i}(\kappa' k'+\kappa k)\chi]\begin{pmatrix} J & 1 & J' \\ K & \sigma'' & K'\end{pmatrix}(-1)^{\frac{\kappa'+1}{2}k'+\frac{\kappa+1}{2}k+J'+p'+K'}$$
$$+\exp[\mathrm{i}(-\kappa' k'-\kappa k)\chi]\begin{pmatrix} J & 1 & J' \\ -K & \sigma'' & -K'\end{pmatrix}(-1)^{\frac{\kappa'+1}{2}k'-\frac{\kappa+1}{2}k+J+p+K}$$
$$+\exp[\mathrm{i}(\kappa' k'-\kappa k)\chi]\begin{pmatrix} J & 1 & J' \\ -K & \sigma'' & K'\end{pmatrix}$$
$$\left.\times(-1)^{\frac{\kappa'+1}{2}k'-\frac{\kappa+1}{2}k+J'+p'+K'+J+p+K}\right]. \tag{37}$$

Next, we expand the sum over σ'' explicitly

$$\langle\Phi'|\mu_s^{(1,\sigma)}|\Phi\rangle$$
$$=(-1)^{M'}[(2J+1)(2J'+1)]^{1/2}\begin{pmatrix} J & 1 & J' \\ M & \sigma & -M'\end{pmatrix}$$
$$\times\sum_{i',i,i_1,i_2,i_3} a_{i',i_1,i_2,i_3}a_{i,i_1,i_2,i_3}N_{K'k'}(\kappa')^{k'}N_{Kk}(\kappa)^{k}(-1)^{K'+\frac{\kappa'+1}{2}k'+\frac{\kappa+1}{2}k}\frac{1}{2\pi}$$
$$\times\iint \mathrm{d}\Omega\, P_{j'}^{|k'-\kappa' K'|}P_j^{|k-\kappa K|}P_{l'}^{k'}P_l^{k}$$
$$\times\left\{\exp[\mathrm{i}(-\kappa' k'+\kappa k)\chi]\left[\mu_m^{(1,0)}\begin{pmatrix} J & 1 & J' \\ K & 0 & -K'\end{pmatrix}\right.\right.$$
$$\left.+\mu_m^{(1,-1)}\begin{pmatrix} J & 1 & J' \\ K & -1 & -K'\end{pmatrix}+\mu_m^{(1,1)}\begin{pmatrix} J & 1 & J' \\ K & 1 & -K'\end{pmatrix}\right].$$
$$+\exp[\mathrm{i}(\kappa' k'+\kappa k)\chi](-1)^{J'+p'+K'}$$
$$\times\left[\mu_m^{(1,0)}\begin{pmatrix} J & 1 & J' \\ K & 0 & K'\end{pmatrix}+\mu_m^{(1,-1)}\begin{pmatrix} J & 1 & J' \\ K & -1 & K'\end{pmatrix}\right.$$
$$\left.+\mu_m^{(1,1)}\begin{pmatrix} J & 1 & J' \\ K & 1 & K'\end{pmatrix}\right]+\exp[\mathrm{i}(-\kappa' k'-\kappa k)\chi](-1)^{J+p+K}$$
$$\times\left[\mu_m^{(1,0)}\begin{pmatrix} J & 1 & J' \\ -K & 0 & -K'\end{pmatrix}+\mu_m^{(1,-1)}\begin{pmatrix} J & 1 & J' \\ -K & -1 & -K'\end{pmatrix}\right.$$
$$\left.\times+\mu_m^{(1,1)}\begin{pmatrix} J & 1 & J' \\ -K & 1 & -K'\end{pmatrix}\right]$$
$$+\exp[\mathrm{i}(\kappa' k'-\kappa k)\chi](-1)^{J'+p'+K'+J+p+K}$$
$$\times\left[\mu_m^{(1,0)}\begin{pmatrix} J & 1 & J' \\ -K & 0 & K'\end{pmatrix}+\mu_m^{(1,-1)}\begin{pmatrix} J & 1 & J' \\ -K & -1 & K'\end{pmatrix}\right.$$
$$\left.\left.\times+\mu_m^{(1,1)}\begin{pmatrix} J & 1 & J' \\ -K & 1 & K'\end{pmatrix}\right]\right\}. \tag{38}$$

Now we can write the expectation value of the dipole moment function in a compact form

$$\langle\Phi'|\mu_s^{(1,\sigma)}|\Phi\rangle$$
$$=(-1)^{M'}[(2J+1)(2J'+1)]^{1/2}\begin{pmatrix} J & 1 & J' \\ M & \sigma & -M'\end{pmatrix}X(J,J'), \tag{39}$$

where $X(J, J')$ does not depend on M, M' and σ. Therefore the line strength is

$$S_{(f\leftarrow i)}=\sum_{M,M',\sigma}|\langle\Phi'|\mu_s^{(1,\sigma)}|\Phi\rangle|^2=(2J+1)(2J'+1)\,|X^2(J,J')|^2$$
$$\times\sum_{\sigma=-1}^{1}\sum_{M}\begin{pmatrix} J & 1 & J' \\ M & \sigma & -(M+\sigma)\end{pmatrix}^2. \tag{40}$$

Since J' can only be equal to J or $J\pm1$, let us consider three different cases:

Case I: $J'=J\leftarrow J$ i.e. $\Delta J=0$. There are three sub-cases:
$\sigma=0$ hence $M=-J\ldots J$,
$\sigma=+1$ hence $M=-J\ldots J-1$,
$\sigma=-1$ hence $M=-J+1\ldots J$
and in any case $\sum_{\sigma=-1}^{1}\sum_M(\ldots)^2=1$. Therefore $S=(2J+1)^2\,X^2(J,J)$.

Case II: $J'=J+1\leftarrow J$ i.e. $\Delta J=1$. There are also three sub-cases:
$\sigma=0$ hence $M=-J\ldots J$,
$\sigma=+1$ hence $M=-J\ldots J$,
$\sigma=-1$ hence $M=-J\ldots J$
and again in any case $\sum_{\sigma=-1}^{1}\sum_M(\ldots)^2=1$. Therefore $S=(2J+1)(2J+3)X^2(J,J')$.

Case III: $J'=J-1\leftarrow J$ i.e. $\Delta J=-1$. This case must be the same as Case II by symmetry (reversibility).

Using the symmetry properties of 3*J*-symbols, we can simplify the line strength expression to obtain

$$S_{(f\leftarrow i)}=(2J+1)(2J'+1)|X(J,J')|^2,\qquad J'=J-1,J,J+1, \tag{41}$$

where

$$X(J,J')=\sum_{i',i,i_1,i_2,i_3}a_{i',i_1,i_2,i_3}a_{i,i_1,i_2,i_3}N_{K'k'}(\kappa')^{k'}N_{Kk}(\kappa)^{k}$$
$$\times(-1)^{K'+\frac{\kappa'+1}{2}k'+\frac{\kappa+1}{2}k}\frac{1}{2\pi}\iint\mathrm{d}\Omega\,P_{j'}^{|k'-\kappa' K'|}P_j^{|k-\kappa K|}P_{l'}^{k'}P_l^{k}$$
$$\times\left\{\mu_m^{(1,0)}\left(\exp[\mathrm{i}(\kappa' k'+\kappa k)\chi](-1)^{J'+p'+K'}\right.\right.$$
$$\left.+\exp[-\mathrm{i}(\kappa' k'+\kappa k)\chi](-1)^{J+p+K+J+1+J'}\right)\begin{pmatrix} J & 1 & J' \\ K & 0 & K'\end{pmatrix}$$
$$+\mu_m^{(1,0)}(\exp[\mathrm{i}(-\kappa' k'+\kappa k)\chi]+\exp[-\mathrm{i}(-\kappa' k'+\kappa k)\chi]$$
$$\times(-1)^{J'+p'+K'+J+p+K+J+1+J'})\begin{pmatrix} J & 1 & J' \\ K & 0 & -K'\end{pmatrix}$$
$$+\left(\mu_m^{(1,1)}\exp[\mathrm{i}(\kappa' k'-\kappa k)\chi](-1)^{J'+p'+K'+J+p+K}+\mu_m^{(1,-1)}\right.$$
$$\times\exp[-\mathrm{i}(\kappa' k'+\kappa k)\chi](-1)^{J+1+J'})\begin{pmatrix} J & 1 & J' \\ -K & 1 & K'\end{pmatrix}$$
$$+\left(\mu_m^{(1,1)}\exp[-\mathrm{i}(\kappa' k'+\kappa k)\chi](-1)^{J+p+K}+\mu_m^{(1,-1)}\right.$$
$$\times\exp[\mathrm{i}(\kappa' k'+\kappa k)\chi](-1)^{J'+p'+K'+J+1+J'})\begin{pmatrix} J & 1 & J' \\ -K & 1 & -K'\end{pmatrix}$$
$$+\left(\mu_m^{(1,1)}\exp[\mathrm{i}(\kappa' k'+\kappa k)\chi](-1)^{J'+p'+K'}+\mu_m^{(1,-1)}\right.$$
$$\times\exp[\mathrm{i}(-\kappa' k'+\kappa k)\chi](-1)^{J+p+K+J+1+J'})\begin{pmatrix} J & 1 & J' \\ K & 1 & K'\end{pmatrix}$$
$$+\left(\mu_m^{(1,1)}\exp[\mathrm{i}(-\kappa' k'+\kappa k)\chi]+\mu_m^{(1,-1)}\right.$$
$$\left.\left.\left.\times\exp[\mathrm{i}(-\kappa' k'+\kappa k)\chi](-1)^{J'+p'+K'+J+p+K+J+1+J'}\right)\right.$$
$$\left.\times\begin{pmatrix} J & 1 & J' \\ K & 1 & -K'\end{pmatrix}\right\}. \tag{42}$$

Due to the properties of 3*j*-symbols the terms in the sum above exist only under special conditions. Furthermore, rigorous selection rules allow only transitions between states with different parity, i.e. $p'\neq p$ (e.g. see Bunker and Jensen

[25] p. 417). This can be also verified explicitly using the expressions above and by taking into account that the action of inversion symmetry does not change μ_x and μ_z but changes the sign of μ_y. Now let us consider the above terms in more detail.

Term I exists only if $K'=K=0$

$$\{\ldots\}=(-1)^{J'+p'}\begin{pmatrix}J & 1 & J'\\ 0 & 0 & 0\end{pmatrix}\mu_z \times\left[\cos(\kappa' k'+\kappa k)\chi+\mathrm{i}\sin(\kappa' k'+\kappa k)\chi +(\cos(\kappa' k'+\kappa k)\chi-\mathrm{i}\sin(\kappa' k'+\kappa k)\chi)(-1)^{p'+p+1}\right]. \quad (43)$$

Since $p'\neq p$ then $(-1)^{p'+p+1}=1$ and

$$\{\ldots\}=(-1)^{J'+p'}\begin{pmatrix}J & 1 & J'\\ 0 & 0 & 0\end{pmatrix}\mu_z\, 2\cos(\kappa' k'+\kappa k)\chi. \quad (44)$$

Term II exsits only if $K'=K$

$$\{\ldots\}=\begin{pmatrix}J & 1 & J'\\ K & 0 & -K\end{pmatrix}\mu_z \times\left[\cos(-\kappa' k'+\kappa k)\chi+\mathrm{i}\sin(-\kappa' k'+\kappa k)\chi +(\cos(-\kappa' k'+\kappa k)\chi-\mathrm{i}\sin(-\kappa' k'+\kappa k)\chi)(-1)^{p'+p+1}\right]. \quad (45)$$

Since $p'\neq p$ then $(-1)^{p'+p+1}=1$ and

$$\{\ldots\}=\begin{pmatrix}J & 1 & J'\\ K & 0 & -K\end{pmatrix}\mu_z\, 2\cos(-\kappa' k'+\kappa k)\chi. \quad (46)$$

Term III exists only if $K'=K-1$, i.e. $(-1)^{K'+K}=1$, and $K=1, 2, 3\ldots$ (while $K'=0, 1, 2\ldots$ respectively)

$$\{\ldots\}=\begin{pmatrix}J & 1 & J'\\ -K & 1 & K-1\end{pmatrix}\frac{(-1)^{J'+J+1}}{2^{1/2}} \times\left[(-\mu_x-\mathrm{i}\mu_y)(\cos(\kappa' k'-\kappa k)\chi+\mathrm{i}\sin(\kappa' k'-\kappa k)\chi)(-1)^{p'+p} +(\mu_x-\mathrm{i}\mu_y)(\cos(\kappa' k'-\kappa k)\chi-\mathrm{i}\sin(\kappa' k'-\kappa k)\chi)\right] \quad (47)$$

$$=\begin{pmatrix}J & 1 & J'\\ -K & 1 & K-1\end{pmatrix}\frac{(-1)^{J'+J+1}}{2^{1/2}} \times\left[-\mathrm{i}\mu_y\cos(\kappa' k'-\kappa k)\chi\left((-1)^{p'+p}+1\right) -\mu_x\cos(\kappa' k'-\kappa k)\chi\left((-1)^{p'+p}-1\right). -\mathrm{i}\mu_x\sin(\kappa' k'-\kappa k)\chi\left((-1)^{p'+p}+1\right) +\mu_y\sin(\kappa' k'-\kappa k)\chi\left((-1)^{p'+p}-1\right)\right]. \quad (48)$$

Since $p'\neq p$ then $(-1)^{p'+p}=-1$ and

$$\{\ldots\}=\begin{pmatrix}J & 1 & J'\\ -K & 1 & K-1\end{pmatrix}\frac{(-1)^{J'+J}}{2^{1/2}} \times 2\left[\mu_y\sin(\kappa' k'-\kappa k)\chi-\mu_x\cos(\kappa' k'-\kappa k)\chi\right]. \quad (49)$$

Term IV exists only if $K'=-K+1$ hence either $K=0$ and $K'=1$ or $K=1$ and $K'=0$

$$\{\ldots\}=\begin{pmatrix}J & 1 & J'\\ -K & 1 & K-1\end{pmatrix}\frac{(-1)^{J+p+K}}{2^{1/2}} \times\left[(-\mu_x-\mathrm{i}\mu_y)(\cos(\kappa' k'+\kappa k)\chi-\mathrm{i}\sin(\kappa' k'+\kappa k)\chi) +(\mu_x-\mathrm{i}\mu_y)(\cos(\kappa' k'+\kappa k)\chi+\mathrm{i}\sin(\kappa' k'+\kappa k)\chi) \times(-1)^{p'+p}(-1)^{K'+K+1}\right] \quad (50)$$

$$=\begin{pmatrix}J & 1 & J'\\ -K & 1 & K-1\end{pmatrix}\frac{(-1)^{J+p+K}}{2^{1/2}} \times\left[-\mu_x\cos(\kappa' k'+\kappa k)\chi\left(1-(-1)^{p'+p}\right) -\mathrm{i}\mu_y\cos(\kappa' k'+\kappa k)\chi\left(1+(-1)^{p'+p}\right). -\mu_y\sin(\kappa' k'+\kappa k)\chi\left(1-(-1)^{p'+p}\right) +\mathrm{i}\mu_x\sin(\kappa' k'+\kappa k)\chi\left(1+(-1)^{p'+p}\right)\right]. \quad (51)$$

Since $p'\neq p$ then $(-1)^{p'+p}=-1$ and

$$\{\ldots\}=\begin{pmatrix}J & 1 & J'\\ -K & 1 & K-1\end{pmatrix}\frac{(-1)^{J+p+K}}{2^{1/2}}2 \times\left[-\mu_x\cos(\kappa' k'+\kappa k)\chi-\mu_y\sin(\kappa' k'+\kappa k)\chi\right]. \quad (52)$$

Term V is not zero only if $K'=-K-1$ and therefore cannot exist.

Term VI exists only if $K'=K+1$, i.e. $K=0, 1, 2\ldots$ (while $K'=1, 2, 3\ldots$ respectively)

$$\{\ldots\}=\begin{pmatrix}J & 1 & J'\\ K & 1 & -K-1\end{pmatrix}\frac{1}{2^{1/2}} \times\left[(-\mu_x-\mathrm{i}\mu_y)(\cos(-\kappa' k'+\kappa k)\chi+\mathrm{i}\sin(-\kappa' k'+\kappa k)\chi) +(\mu_x-\mathrm{i}\mu_y)(\cos(-\kappa' k'+\kappa k)\chi-\mathrm{i}\sin(-\kappa' k'+\kappa k)\chi)(-1)^{p'+p}\right] \quad (53)$$

$$=\begin{pmatrix}J & 1 & J'\\ K & 1 & -K-1\end{pmatrix}\frac{1}{2^{1/2}} \times\left[-\mu_x\cos(-\kappa' k'+\kappa k)\chi\left(1-(-1)^{p'+p}\right) -\mathrm{i}\mu_y\cos(-\kappa' k'+\kappa k)\chi\left(1+(-1)^{p'+p}\right) +\mu_y\sin(-\kappa' k'+\kappa k)\chi\left(1-(-1)^{p'+p}\right)-\mathrm{i}\mu_x\sin(-\kappa' k'+\kappa k) \chi\left(1+(-1)^{p'+p}\right)\right]. \quad (54)$$

Since $p'\neq p$ then $(-1)^{p'+p}=-1$ and

$$\{\ldots\}=\begin{pmatrix}J & 1 & J'\\ K & 1 & -K-1\end{pmatrix}\frac{2}{2^{1/2}} \times\left[-\mu_x\cos(-\kappa' k'+\kappa k)\chi+\mu_y\sin(-\kappa' k'+\kappa k)\chi\right]. \quad (55)$$

The projections of the dipole are real functions and therefore $X(J, J')$ is real too.

Let us define $\Delta K=K-K'$, i.e. $K=K'+\Delta K$. The equations can be also summarised in a more compact form for different cases of ΔK and K'.

$\Delta K=0$, $K=K'=0$ (Terms II and I)

$$\{\ldots\}=\begin{pmatrix}J & 1 & J'\\ 0 & 0 & 0\end{pmatrix}\mu_z \times 2\left[\cos(\kappa' k'-\kappa k)\chi+(-1)^{J'+p'}\cos(\kappa' k'+\kappa k)\chi\right]. \quad (56)$$

$\Delta K=0$, $K=K'>0$ (Term II)

$$\{\ldots\}=\begin{pmatrix} J & 1 & J' \\ K' & 0 & -K' \end{pmatrix}\mu_z\, 2\cos(\kappa' k'-\kappa k)\chi. \qquad (57)$$

$\Delta K=1$, $K'=0$, $K=1$ (Terms III and IV)

$$\{\ldots\}=\begin{pmatrix} J & 1 & J' \\ -1 & 1 & 0 \end{pmatrix}2^{1/2} \times\Big[\mu_x\Big((-1)^{J'+J+1}\cos(\kappa' k'-\kappa k)\chi+(-1)^{J+p}\cos(\kappa' k'+\kappa k)\chi\Big) +\mu_y\Big((-1)^{J'+J}\sin(\kappa' k'-\kappa k)\chi+(-1)^{J+p}\sin(\kappa' k'+\kappa k)\chi\Big)\Big]. \qquad (58)$$

$\Delta K=1$, $K'>0$, $K=K'+1$ (Term III)

$$\{\ldots\}=\begin{pmatrix} J & 1 & J' \\ -K'-1 & 1 & K' \end{pmatrix}2^{1/2} \times\Big[\mu_x(-1)^{J'+J+1}\cos(\kappa' k'-\kappa k)\chi \times+\mu_y(-1)^{J'+J}\sin(\kappa' k'-\kappa k)\chi\Big]. \qquad (59)$$

$\Delta K=-1$, $K'=1$, $K=0$ (Terms VI and IV)

$$\{\ldots\}=\begin{pmatrix} J & 1 & J' \\ 0 & 1 & -1 \end{pmatrix}2^{1/2} \times\big[\mu_x\big(-\cos(\kappa' k'-\kappa k)\chi+(-1)^{J+p+1}\cos(\kappa' k'+\kappa k)\chi\big) +\mu_y\big(-\sin(\kappa' k'-\kappa k)\chi+(-1)^{J+p+1}\sin(\kappa' k'+\kappa k)\chi\big)\big]. \qquad (60)$$

$\Delta K=-1$, $K'>1$, $K=K'-1$ (Term VI)

$$\{\ldots\}=\begin{pmatrix} J & 1 & J' \\ K'-1 & 1 & -K' \end{pmatrix}2^{1/2} \times\big[-\mu_x\cos(\kappa' k'-\kappa k)\chi-\mu_y\sin(\kappa' k'-\kappa k)\chi\big]. \qquad (61)$$

The expressions above provided the basis for performing numerical line strength calculations and were used in the new DIPOLE4 code to compute line intensities. In practice, we calculate $X(J, J')$ as a sum of three terms each depending on either μ_x, μ_y or μ_z. The code supplements WAVR4 [22] and was written in Fortran 90 as WAVR4 itself. The code takes as an input a set of initial and final eigenfunctions, a dipole function, and a control file and computes line strengths between all possible combinations of initial and final states. It follows from the equations above that there must be necessarily a sum (i.e. a loop) over all angular and radial basis functions and an integration of the dipole function in order to obtain its matrix representation in the angular basis. We should note again that we assume diagonal representation of the dipole function in the radial basis. Since the basis functions (both FBR and DVR parts) are the same as those used in WAVR4, we could readily use the integration functions from WAVR4 for integration over the angular (FBR) basis and perform direct summation for the integration over the radial grids. For the purposes of the current project we only needed evaluation of matrix elements of the dipole moment function and DIPOLE4 code has been modified accordingly.

One note on the implementation is in order. If the integration-summation formulae are taken literally then they may result in matrix vector multiplication which is very inefficient on cache-based computer architectures for matrices larger than the cache. Therefore we decided to operate simultaneously on several initial and final eigenfunctions and thus utilise matrix–matrix multiplication which is much more efficient. At the core, the new code is essentially a loop over the three-dimensional radial grid which builds a matrix representation of the integrand in the primitive basis and performs computations of integrals involving all possible initial and final states. The intermediate results are accumulated in a matrix of the size equal to the number of initial times final states. The loop over the radial grid lends itself to a very efficient parallelisation strategy. In the parallel implementation, the accumulators reside on every parallel processor so that no communication is necessary during the computation. Only a final reduction is required to gather the intermediate accumulators and compute the transition matrix.

Finally, one additional step is required for the calculation of dipole transitions. The wave-functions produced by WAVR4 need to be transformed back into the primitive basis on which DIPOLE4 operates. This is done using a separate program and the results are stored on disk. The two-step approach allows more efficient calculation of the integrals, reuse of converted wave functions as well as potential use of DIPOLE4 with the codes which do not implement contraction-reduction strategy (e.g. direct methods).